MARTIN MARIETTA ENERGY SYSTEMS LIBRARIES

3 4456 0361080 3

ORNL/TM-11999

ornl

OAK RIDGE
NATIONAL
LABORATORY

MARTIN MARIETTA

Long-Reach Manipulation for Waste Storage Tank Remediation

FY 1991 Report

J. F. Jansen
S. March-Leuba
D. S. Kwon
S. M. Babcock
B. L. Burks
R. L. Kress
W. R. Hamel

OAK RIDGE NATIONAL LABORATORY
CENTRAL RESEARCH LIBRARY
CIRCULATION SECTION
4500N ROOM 175
LIBRARY LOAN COPY
DO NOT TRANSFER TO ANOTHER PERSON
If you wish someone else to see this report, send in name with report and the library will arrange a loan.

rpsd

MANAGED BY
MARTIN MARIETTA ENERGY SYSTEMS, INC.
FOR THE UNITED STATES
DEPARTMENT OF ENERGY

This report has been reproduced directly from the best available copy.

Available to DOE and DOE contractors from the Office of Scientific and Technical Information, P.O. Box 62, Oak Ridge, TN 37831; prices available from (615) 576-8401, FTS 626-8401.

Available to the public from the National Technical Information Service, U.S. Department of Commerce, 5285 Port Royal Rd., Springfield, VA 22161.

This report was prepared as an account of work sponsored by an agency of the United States Government. Neither the United States Government nor any agency thereof, nor any of their employees, makes any warranty, express or implied, or assumes any legal liability or responsibility for the accuracy, completeness, or usefulness of any information, apparatus, product, or process disclosed, or represents that its use would not infringe privately owned rights. Reference herein to any specific commercial product, process, or service by trade name, trademark, manufacturer, or otherwise, does not necessarily constitute or imply its endorsement, recommendation, or favoring by the United States Government or any agency thereof. The views and opinions of authors expressed herein do not necessarily state or reflect those of the United States Government or any agency thereof.

ORNL/TM -11999

LONG–REACH MANIPULATION FOR WASTE STORAGE TANK REMEDIATION FY 1991 REPORT

J. F. JANSEN, S. MARCH-LEUBA, D. S. KWON, S. M. BABCOCK,
B. L. BURKS, R. L. KRESS, AND W. R. HAMEL
ROBOTICS & PROCESS SYSTEMS DIVISION

Date Published–March 1992

NOTICE This document contains information of a preliminary nature. It is subject to revision or correction and therefore does not represent a final report.

Prepared by the
OAK RIDGE NATIONAL LABORATORY
Oak Ridge, Tennessee 37831
managed by
MARTIN MARIETTA ENERGY SYSTEMS, INC.
for the
U.S. DEPARTMENT OF ENERGY
under contract DE-AC05-84OR21400

MARTIN MARIETTA ENERGY SYSTEMS LIBRARIES
3 4456 0361080 3

CONTENTS

Page

ABSTRACT 1

1. INTRODUCTION 2

2. WASTE TANK REMEDIATION BACKGROUND 3
   - 2.1 CURRENT DOE WASTE TANK REMEDIATION EFFORTS 3
   - 2.2 FISCAL YEAR 1991 WASTE TANK REMEDIATION DEMONSTRATION AT HANFORD 4

3. SIMPLIFIED MODELS AND BASIC LIMITATIONS OF STRUCTURAL ELEMENTS 7
   - 3.1 DIFFERENCES BETWEEN CONVENTIONAL MANIPULATORS AND LONG-REACH MANIPULATORS 7
   - 3.2 DEFLECTION AND NATURAL FREQUENCIES 7
   - 3.3 LIMITATIONS WITH ACTIVE CONTROL 11
   - 3.4 ISSUE OF COMPOSITE MATERIALS FOR CONSTRUCTION 13

4. ANALYSIS OF WORKSPACE REQUIREMENTS 14
   - 4.1. IMPACT OF THE NUMBER OF ACCESS PORTS 14
   - 4.2. OTHER IMPACTS ON THE SELECTION OF A MANIPULATOR KINEMATIC DESIGN FOR WASTE TANK REMEDIATION 17

5. LITERATURE SURVEY ON THE CONTROL OF FLEXIBLE MANIPULATORS AND STRUCTURES 18
   - 5.1 INTRODUCTION 18
   - 5.2 OPEN-LOOP TRAJECTORY PLANNING 18
     - 5.2.1 Vibration Suppression 18
     - 5.2.2 Inverse Dynamic Methods 19
   - 5.3 TRAJECTORY FOLLOWING USING SENSORY FEEDBACK 20
     - 5.3.1 Nonadaptive Control 20
     - 5.3.2 Beam Redesign and Torque Transmission Relocation 22
     - 5.3.3 Adaptive and Robust Control 22
     - 5.3.4 High-Performance End-effector for Dynamic Compensation 24
     - 5.3.5 Repetitive Control System 24
   - 5.4 MULTIPLE CONTROL STRATEGIES 24
     - 5.4.1 Bracing Strategies 24
     - 5.4.2 Contact Control 25

Page

6. MODELING OF SINGLE LINK FLEXIBLE STRUCTURES 26
   6.1 A TRANSFER FUNCTION APPROACH 26
      6.1.1 Model Development 26
      6.1.2 Product Expansions for Transfer Function Models 31
         6.1.2.1 Analytic and Numeric Issues 31
         6.1.2.2 Listing of Normalized Transfer Function 33
         6.1.2.3 Explicit Transfer Function 40
      6.1.3 Simulation Method 41
   6.2 MODELING OF A FLEXIBLE MANIPULATOR USING MODAL ANALYSIS 43
   6.3 COMPARISON OF EXACT MODEL WITH MODAL-BASED MODEL 44

7. OPEN-LOOP TRAJECTORY PLANNING 46
   7.1 BASIC APPROACHES 46
   7.2 INVERSE DYNAMICS METHOD 46

8. FLEXIBLE MANIPULATOR CONTROL 51
   8.1 SUMMARY OF BASIC CONTROL APPROACHES 51
   8.2 SENSOR TYPE AND LOCATION DISCUSSION 51
   8.3 CLASSICAL CONTROLLER DESIGN 51
      8.3.1 Plant and Controller Model 51
      8.3.2 Inner Loop Design 52
      8.3.3 Outer Loop Design 53
   8.4 SUMMARY AND CONCLUSION 57

9. KINEMATIC OPTIONS FOR MULTI-DEGREE-OF-FREEDOM MANIPULATORS 58
   9.1 JOINT ACTUATION 58
   9.2 DRIVE LINKAGE STUDIES 58
      9.2.1 Analysis 59
      9.2.2 Conclusion 62
   9.3 SIMPLE STRUCTURES APPROACHES - A COMPARISON OF WORKSPACES 63
      9.3.1 Optimization of the Workspace of a Revolute Joint Robot 63
      9.3.2. RPP Manipulator Workspace Optimization 64
         9.3.2.1 Workspace as a Function of Angular Constraints and Lengths 64
         9.3.2.2 Area and Volume Covered by an RPP Manipulator 68
         9.3.2.3 Elbow Up, Elbow Down on an RPP Manipulator 69

Page

9.3.2.4 Conclusions for an RPP Manipulator Optimization 70
9.3.3. RPE Manipulator Workspace Optimization....72
9.3.3.1 Two and Three Stages for an RPE Manipulator....73
9.3.3.2 Conclusions for RPE Manipulator Optimization 75
9.3.4. RPPE Manipulator Workspace 77
9.3.4.1 Graphical Analysis of Workspace....77
9.3.4.2 Conclusions for RPPE Manipulator Optimization 78
9.3.5 Conclusions of the Kinematic Configuration Study....79
9.4 OTHER CONSIDERATIONS CONCERNING FUNDAMENTAL KINEMATIC CONSIDERATIONS....80

10. CONCLUSIONS AND FUTURE DIRECTIONS....82

11. REFERENCES....85

LIST OF FIGURES

Figure Page

2.1 Spar RMS 2500 manipulator 6

3.1 Clamped-free beam 7

3.2 Beam pinned at the center 10

4.1 Length of manipulator required for various numbers of tank access ports 15

4.2 Optimized locations of waste tank ports 16

6.1 Beam parameters 27

6.2 Cascading of filter for simulation of product expansion 41

7.3 Location of the Br contour for the d = 2 case 49

8.1 Block diagram of flexible beam and classical controller 52

8.2 Inverse polar plot of $G_{in}(s)$ with $K_v^{\theta} = 12$ 53

8.3 Open-loop transfer function 54

8.4 Kp = 5.5 and Kv = 1 55

8.5 Kp = 4 and Kv = 1 56

8.6 Ramped response 56

9.1 Joint linkage configuration for a hydraulic cylinder 59

9.2 Maximum range of the joint angle motion
X axis : L2, Y axis : L3, Z axis: joint angle range (degrees) 61

9.3 Joint torque distribution
X axis: L1 (hydraulic cylinder length),
Y axis: L2,
Z axis: Torque arm length. 61

Figure Page

9.4 Joint torque for different linkage configurations
X axis: L1 (hydraulic cylinder actuator),
Y axis: torque arm length 62

9.5 Symmetric workspace of a robot with an initial rotational joint 64

9.6 Two-link, planar, revolute joint robot to which an RPP robot can be reduced to study its workspace 65

9.7 Two different points of view of the area of the workspace of an RPP robot as a function of the relation between its lengths and its angular constraints 66

9.8 Area of an RPP manipulator with L1 = L2 as a function of the angular range constraints 67

9.9 Workspace of an RPP robot when L1 = L2 and $(\theta_{1max} - \theta_{1min}) = (\theta_{2max} - \theta_{2min}) = 140°$ 69

9.10 Workspace of an RPP robot when L1 = L2, $(\theta_{1max} - \theta_{1min}) = 140°$, and $(\theta_{2max} - \theta_{2min}) = 280°$ 70

9.11 Workspace of an RPP robot when L1 = L2 and three discrete positions for the shoulder at (0,.25), (0, -.25), and (0,-.75), and the height of the tank equal to 1 71

9.12 An RPP robot with the elbow up and down 72

9.13 Workspace of an RPP robot when L1 = L2, three discrete positions for the shoulder at (0,.25), (0, -.40), and (0,-.70) and the height of the tank is equal to 1 73

9.14 One link planar extension robot to which an RPE robot can be reduced to study its workspace 74

9.15 Workspace of an RPE robot with two stages and three discrete positions for the shoulder at (0,.25), (0, -.25), and (0,-.75), given a tank height of 1 75

9.16 Workspace of an RPE robot with three stages and three discrete positions for the shoulder at (0,.25), (0, -.25), and (0,-.75), given a tank eight of one 76

Figure Page

9.17 Three-link planar robot to which an RPPE robot can be reduced to study its workspace 78

9.18 Workspace of an RPPE robot with three stages for the second link and two discrete positions for the shoulder at (0, .25) and (0, -.25) and the height of the tank is equal to 1 79

LIST OF TABLES

Table Page

3.1a Steel 9

3.1b Aluminum 9

3.1c Titanium 9

3.2 Material properties 10

3.3 Natural frequency of steel beam 10

3.4 Natural frequency of steel beam pinned at center 11

4.1 Rate of change of manipulator length with number of access ports 15

6.1 Pole locations for all transforms 33

6.2a H_u^y zero locations ($\xi = 1$ and $K_{dc} = 1$) 33

6.2b H_u^y zero locations ($\xi = 0.9$ and $K_{dc} = 1$) 34

6.2c H_u^y zero location ($\xi = 0.8$ and $K_{dc} = 1$) 34

6.2d H_u^y zero location ($\xi = 0.7$ and $K_{dc} = 1$) 35

6.2e H_u^y zero location ($\xi = 0.6$ and $K_{dc} = 1$) 35

6.2f H_u^y zero location ($\xi = 0.5$ and $K_{dc} = 1$) 36

6.2g H_u^y zero location ($\xi = 0.4$ and $K_{dc} = 1$) 36

6.2h H_u^y zero location ($\xi = 0.3$ and $K_{dc} = 1$) 37

6.2i H_u^y zero location ($\xi = 0.2$ and $K_{dc} = 1$) 37

6.2j H_u^y zero location ($\xi = 0.1$ and $K_{dc} = 1$) 38

Table | Page

6.3. H_f^y zero location ($\xi = 1$ and $K_{dc} = 1$) 38

6.4 H_m^y zero location ($\xi = 1$ and $K_{dc} = 1$) 39

6.5 H_u^m zero location ($\xi = 0.5$ and $K_{dc} = 1$) 39

6.6 H_u^θ zero location ($\xi = 0$ and $K_{dc} = 1$) 40

6.7 A comparison of poles for joint torque input and end-point position output 45

6.8 A comparison of zeros for joint torque input and end-point position output 45

9.1 Joint angle range vs L2 and L3 60

9.2 Percent change in workspace area 67

ABSTRACT

Remediation of large underground storage tanks containing hazardous waste provides an application for state-of-the-art technology in flexible link manipulator design and control and indicates a need for additional research and development. Application requirements are described, and preliminary analyses associated with this problem are summarized. Inherent physical limitations of flexible manipulators are discussed. Potential kinematic configurations, drive-train elements, and control issues for both free-space motion and damping of forced vibration are addressed. Also included are future directions for research and development in mechanical components and control strategies.

1. INTRODUCTION

Remediation of large underground storage tanks containing hazardous waste provides an application for state-of-the-art technology in flexible link manipulator design and control and indicates a need for additional research and development. This report describes work conducted in FY 1991 on the long reach manipulation problem. Chapter 2 provides a brief background on the waste tank remediation problem and summarizes a demonstration sponsored by the Department of Energy's (DOE's) Environmental Restoration and Waste Management Office of Technology Development conducted at Hanford. Chapter 3 covers the basic analysis of flexible structures including the deflection and first mode natural frequency of a clamped-free beam. Also included are discussions of basic limitations associated with active control and the issue of composite materials. Chapter 4 provides a preliminary analysis of the workspace requirements focusing on the impact of the number of access ports. Other impacts on the selection of a manipulator kinematic design are briefly discussed. Chapter 5 provides a survey of the literature associated with the control of manipulators with flexible links. In Chapter 6, a transfer function approach to modeling and simulation of flexible structures is developed, a modal analysis approach is described, and a comparison of the two is provided. In Chapter 7, various approaches to open-loop trajectory planning are discussed with a particular focus on the inverse dynamics method. Chapter 8 covers basic control approaches for flexible manipulators, discusses the possible sensors to be used and their locations, and provides a classical controller design. Chapter 9 includes a brief discussion of joint actuation options and an analysis of the range of motion of revolute joints which is practical with linear actuators; however, the primary focus is on a comparison of the positioning workspaces of three potential kinematic configurations. In addition, other considerations in the selection of a kinematic configuration are briefly discussed. Chapter 10 provides some conclusions that have been drawn and briefly discusses future directions.

2. WASTE TANK REMEDIATION BACKGROUND

Since the late 1940s and early 1950s one of the primary missions of DOE and its predecessor agencies, the Atomic Energy Commission and the U.S. Energy Research and Development Administration, has been the production of strategically important radioactive materials. In addition to the operation of production facilities, numerous facilities were established to research material properties and to develop the technology required to utilize the radioactive products. Each production or research facility handling radioactive materials generated waste by-products that were also radioactive or contaminated by radioactive materials. One of the most common disposal approaches for liquid and sludge waste streams was storage in large, single-shell, steel, underground storage tanks or in large, reinforced concrete above ground silos. This approach was viewed as a temporary solution since the storage tanks were typically designed for 20- to 50-year life cycles. Unfortunately, many of these storage tanks are still in use and have developed leaks.

2.1 CURRENT DOE WASTE TANK REMEDIATION EFFORTS

DOE is currently engaged in an aggressive effort to reduce the generation of radioactive waste by-products and to remediate contaminated sites and facilities. One of the highest priority remediation areas is waste storage tanks–in particular, those suspected of, or documented as, leaking. Many of the concepts envisioned for deployment of remediation tools in waste storage tanks rely on long-reach, high-capacity manipulator systems. Discussed in this paper, in general terms, are the physical constraints, performance needs, and control issues related to use of long-reach manipulators for remediation of typical waste storage tanks found in the DOE complex.

Hundreds of waste storage tanks are in the DOE complex. Most of the older tanks are single-shell steel tanks, whereas most of the newer tanks are double-shell for added containment protection. It is very difficult to describe a typical waste storage tank in the DOE complex because the physical properties of these tanks and their contents vary greatly from site to site. The largest tanks and concrete silos are 75 to 80 ft in diameter, approximately 35 ft high, cylindrical, and have dome-shaped tops. Access to the interior of the tanks is usually through a limited number of circular penetrations in the dome ranging in diameter from 12 in. for tanks at the Idaho National Engineering Laboratory (INEL), Idaho Falls, Idaho, to 42 in. for some tanks at the Hanford site, Richland, Washington. The K-65 waste silos at the Feed Materials Production Center, Fernald, Ohio, are constructed of reinforced concrete and have access ports that are only 20 in. in diameter.

Radiation exposures at the tank waste surfaces throughout the complex vary from a few millirem per hour to hundreds of rem per hour. The pH level of waste material can be highly acidic for some tanks and highly alkaline for others (e.g., the pH level is 12 in some tanks at INEL). The waste forms include liquids, sludges, crusts, and hardpan. Some of the waste could be easily dissolved in water and removed through hydraulic pumping or mining. At other sites the liquid content was decanted years ago leaving a solid waste that has dried as hard as concrete; this type of waste requires much greater effort to mobilize and to retrieve. Remediation concepts vary from simple scoop or clam-shell devices to devices like jackhammers and scabblers that generate large reaction forces on the deployment system.

At present, nearly every waste storage tank remediation project is still in the planning stage (i.e., accurate characterization of wastes and design of appropriate retrieval approaches). Because a huge investment will be made in engineering, design, fabrication, and operation of the systems that eventually remediate the large number of DOE waste storage tanks, this is an appropriate time to perform trade-off analyses between remediation requirements and both current and near-term manipulator technology.

2.2 FISCAL YEAR 1991 WASTE TANK REMEDIATION DEMONSTRATION AT HANFORD

During the summer of 1991, DOE's Environmental Restoration and Waste Management Office of Technology Development sponsored a series of technology demonstrations focusing on applications of robotics technology in waste cleanup needs. A demonstration of technology applicable to characterization and remediation of wastes stored in large underground tanks took place at the Hanford site. Oak Ridge National Laboratory (ORNL) is one of four DOE laboratories that provided equipment and expertise for this demonstration. Others include the INEL, Pacific Northwest Laboratory, and Sandia National Laboratories. Remotely operated equipment from the four laboratories and from Hanford were brought together at Hanford where a 45° mock storage tank sector was constructed for the demonstration. The primary ORNL contribution to the test facility was a telerobotic manipulator with a 28-ft reach, a 2500-lb lift capacity, and a 0.05-in. positioning accuracy that serves as the long-reach, high-capacity boom required for initial positioning of an attached dextrous manipulator and end effector tools. ORNL also provided an optical proximity sensor and control software for surface following and close-range mapping.

Although the eventual remediation system will require deployment from an overhead bridge, for the FY 1991 test facility ORNL utilized an existing floor-mounted manipulator for the test stand boom. A lease

agreement was arranged for use of a reassembled and refurbished Spar RMS 2500 manipulator system (see Fig. 2.1) developed by Spar Aerospace Limited for Ontario Hydro. This manipulator system was designed for maintenance of Candu reactors and hence has many features also required for waste tank remediation (e.g., redundant actuators and radiation-hardened computers and electronics) in addition to long-reach, high-positioning accuracy and high lift capacity. ORNL developed a controller for the Spar manipulator that permits operation from either a local control station or from the master control station for the integrated demonstration. The Spar manipulator system was installed at Hanford in late May. Final development and testing of the ORNL controller, together with integration with other sensors, robots, end effectors, and the master controller, took place in June. The integrated system became fully operational by the multi-laboratory team in late July.

ORNL-PHOTO 9817-91

Fig. 2.1. Spar RMS 2500 manipulator.

3. SIMPLIFIED MODELS AND BASIC LIMITATIONS OF STRUCTURAL ELEMENTS

3.1 DIFFERENCES BETWEEN CONVENTIONAL MANIPULATORS AND LONG-REACH MANIPULATORS

Conventional manipulators, especially those that have been built by ORNL, have typically had a 6-ft reach. Dynamic models have typically been lumped parameter models for rigid bodies with the major compliance emanating from the drive trains because of torsional loading. The energy storage of the drive system is predominantly potential energy because of the low inertia in the drive train, thus simple spring models have been adequate. A long-reach manipulator with a large aspect ratio (length to diameter) is a fundamentally different problem. Energy storage for this type of manipulator is distributive by nature because of the potential energy resulting from bending and the kinetic energy due to deflection rates. Instead of ordinary differential equations, partial differential equations result, making the analysis more challenging. Some of the inherent physical limitations are discussed in this section.

3.2 DEFLECTION AND NATURAL FREQUENCIES

The 30-ft boom (with a high-aspect ratio) has very low structural frequencies. A simple clamped-free beam was examined to obtain a basic "feel" for the amount of deflection and the magnitude of the natural frequency for the first wave mode of transverse vibration without resorting to finite-element analysis. This type of analysis excludes the effects of drive-train and controller compliance and therefore gives best-case values. Drive-train and controller compliance are discussed later. Figure 3.1 shows the clamped-free beam with length L.

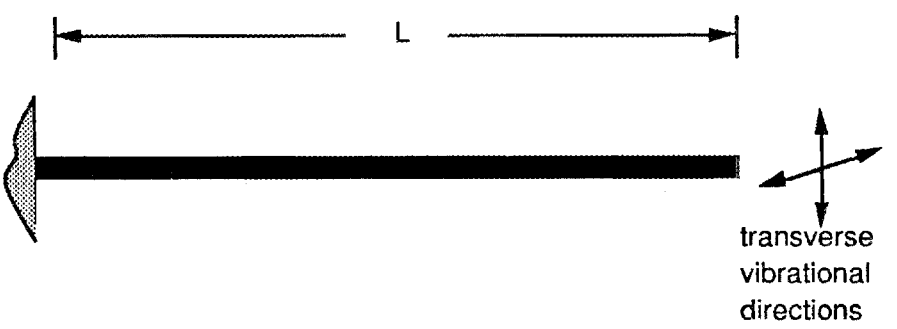

Fig. 3.1. Clamped-free beam.

The maximum static beam deflection, δ_{max}, can be partitioned into two components. The first is the deflection due only to the weight of the beam; the second is due to the static load forces **[Higdon,76]** which can be written as

$$\delta_{max} = \delta^{w}_{max} + \delta^{P}_{max} , \tag{3.1}$$

where

$\delta^{w}_{max} = -\dfrac{w L^4}{8 E I}$ = static deflection due to beam weight,

$\delta^{P}_{max} = -\dfrac{P L^3}{3 E I}$ = static deflection due to static load forces,

w = weight of arm per unit length,
P = static load at end of beam,
L = total length of beam,
E = modulus of elasticity,
I = cross-sectional inertia.

Assuming a uniform beam cross section, we find that deflection due to the beam weight can be rewritten as

$$\delta^{w}_{max} = -\frac{L^4}{8\left(\frac{E}{\rho}\right)\left(\frac{I}{A}\right)} , \tag{3.2}$$

where

A = cross-sectional area of beam,
ρ = material density.

Equation (3.2) has the factor E/ρ, which is fairly constant over a wide range of materials such as steel, aluminum, and titanium. Also, the I/A factor in Eq. (3.22) has a least upper bound for a circular cross-sectional area and can be shown to be

$$\frac{I}{A} = \frac{r^2_{max} + (r_{max} - t)^2}{4} < \frac{r^2_{max}}{2} , \tag{3.3}$$

where

r_{max} = maximum radius of the beam,
t = thickness of cross section.

Therefore, the lower bound for the deflection due to the beam weight can be written in a form that is for all practical purposes independent of materials and beam thickness:

$$\delta_{max}^{w} > -\frac{L^4}{8\left(\frac{E}{\rho}\right)\left(\frac{r_{max}^2}{2}\right)} = \tilde{\delta}_{max}^{w} , \tag{3.4}$$

where $\tilde{\delta}_{max}^{w}$ is the lower bound of the deflection due to the beam weight.

For a beam length of 30 ft (a typical length being considered for use in waste tank remediation), the static deflections shown in Tables 3.1a through 3.1c can be determined.

Table 3.1a. Steel

r_{max} (in.)	t (in.)	δ_{max}^{w} (in.)	$\tilde{\delta}_{max}^{w}$ (in.)	P (lb)	δ_{max}^{P} (in.)	δ_{max} (in.)
15	1	0.19	0.17	1000	0.05	0.24
15	1	0.19	0.17	2000	0.11	0.29
10	1	0.43	0.39	1000	0.19	0.62
10	1	0.43	0.39	2000	0.38	0.81

Table 3.1b. Aluminum

r_{max} (in.)	t (in.)	δ_{max}^{w} (in.)	$\tilde{\delta}_{max}^{w}$ (in.)	P (lb)	δ_{max}^{P} (in.)	δ_{max} (in.)
15	1	0.19	0.19	1000	0.17	0.36
15	1	0.19	0.19	2000	0.33	0.52
10	1	0.45	0.42	1000	0.58	1.03
10	1	0.45	0.42	2000	1.15	1.60

Table 3.1c. Titanium

r_{max} (in.)	t (in.)	δ_{max}^{w} (in.)	$\tilde{\delta}_{max}^{w}$ (in.)	P (lb)	δ_{max}^{P} (in.)	δ_{max} (in.)
15	1	0.21	0.19	1000	0.11	0.32
15	1	0.21	0.19	2000	0.21	0.42
10	1	0.49	0.44	1000	0.38	0.87
10	1	0.49	0.44	2000	0.75	1.24

The material properties are given in Table 3.2.

Table 3.2. Material properties

Materials	E Modulus of elasticity (1000 ksi)	ρ Specific weight (lb/in.^{3})
Steel	30.0	0.28
Aluminum	10.0	0.10
Titanium	15.4	0.16

The natural frequency in hertz for the first wave mode of transverse vibrations can be expressed as

$$f_{T1} = \frac{\lambda_1^2}{2\pi L^2}\left[\left(\frac{E}{\rho}\right)\left(\frac{I}{A}\right)\right]^{1/2}, \tag{3.5}$$

where λ_1 = 1.85 = eigenvalue for the first wave mode. Equation (3.5) in a slightly modified form can be found in **[Blevins,79]**. Equation (3.5) is written in a form that is basically independent of material. Using the upper bound for the I/A factor, one can determine the natural frequency for the first transverse vibration wave mode for a 30-ft steel beam (Table 3.3).

Table 3.3. Natural frequency of steel beam

r_{max} (in.)	f_{T1} (Hz)
15	9.07
10	6.05

If the beam is pinned at its center (Fig. 3.2), the natural frequencies will obviously change. Pinning the beam at the center could be accomplished by means of a truss assembly.

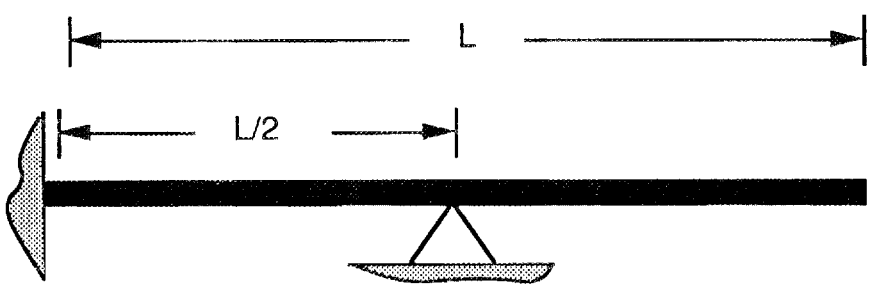

Fig. 3.2. Beam pinned at the center.

A formula similar to Eq. (3.5) can be determined **[Blevins,79]** and is simply

$$f_{T1} = \frac{4\,\lambda_1^2}{2\,\pi\,L^2}\left[\left(\frac{E}{\rho}\right)\left(\frac{I}{A}\right)\right]^{1/2}, \tag{3.6}$$

where $\lambda_1 = 1.57$. Equation (3.6) is again written in a form that is basically independent of material. Using the upper bound for the I/A factor, one can determine the natural frequency for the first transverse vibration wave mode for a 30-ft steel beam (Table 3.4).

Table 3.4. Natural frequency of steel beam pinned at center

r_{max} (in.)	f_{T1} (Hz)
15	26.13
10	17.42

Tapering the beam can raise the value of the natural frequency by roughly a factor of 2 **[Blevins,79]**. Also, changing the cross section to that of an I beam will not improve the situation because the I/A ratio will improve in one direction at the expense of the other transverse vibration direction.

This analysis excluded the effects of drive train and controller compliance and therefore gave best-case values. Even if the boom was just a collection of welded pipes, the boom would have low natural frequencies and significant deflection. While the Spar RMS 2500 series manipulator cannot access the interior of any of the waste tanks because of its large cross section, it is still useful to compare its natural frequency with the above simple analysis. The Spar has a natural frequency of about 0.7 Hz; this indicates that the effects of drive train and controller compliance will be extremely important.

3.3 LIMITATIONS WITH ACTIVE CONTROL

Using a Bernoulli-Euler beam model, one may describe the flexible deflections by a finite series of assumed modes with respect to a reference frame. Linear, time-invariant models for the flexible beam are frequently derived and give fair agreement with experimental data **[Hastings,86]**. Typically, the first two wave modes are used in a truncated modal analysis. More elaborate beam models such as the Timoshenko's beam model are usually in good agreement with the Bernoulli-Euler beam model at low frequencies **[Weaver,90]**. Developed by numerous researchers, these linear, time-invariant models and their associated properties follow:

1. A collocated system (i.e., one where the actuator and sensor are located together) has alternating pole/zero pairs along the imaginary axis **[Miu,90]**.

2. A noncollocated system (i.e., one where the actuator and sensor are separated by a finite distance) will not necessarily have alternating pole/zero pairs; this will cause severe phase lag problems. Further, zeros can appear on the right half plane creating a nonminimum phase condition **[Spector,90]**.
3. Small variations in sensor location can result in qualitatively different system characteristics producing significant phase errors of up to -360° **[Spector,90]**.
4. Transfer functions for noncollocated systems are always nonminimum phase beyond some finite frequency **[Spector,90]**.

Drive trains are most likely to be either hydraulic or electric. Hydraulic drive trains have a greater power-to-weight ratio than electric drive trains but are more difficult to use. If hydraulic drive trains are chosen, the accuracy of a linearized model will be questionable because of the inherent square-root relationship between pressure and flow and dissipative forces that vary nonlinearly as a function of servo valve amplitude **[Merritt,67]**. If electric drive trains are chosen, large gear/transmission ratios will be required because of the 1000- to 2000-lb payload plus the boom weight. Large gear/transmission ratios result in large nonlinear frictional forces and nonlinear compliance effects **[Good,85]**. Again, accurate models will be difficult if not impossible to obtain.

Based on the above discussion, model-based control methods will be difficult to apply to the long-reach boom. Off-line techniques that generate joint trajectories having minimum end-effector trajectory error **[Mecki,90]** could be utilized along with robust types of controllers based on sensory feedback to damp out residual vibrations. Servo bandwidths must be set below the first modal frequency. Bandwidths below 67% of the first wave mode frequency **[Cetinkunt,90a]** are inherent limits. With PD-type controllers, a practical bandwidth limit of 20 to 33% of first wave mode is used. For example, considering the Spar RMS 2500 manipulator, one finds that the servo bandwidth was limited to 33% of the first wave mode frequency. Robust schemes that can switch from positional control to force control will be examined.

The above discussion is only relevant for a beam of fixed length but can be extended to multiple links with revolute joints. While researchers of flexible manipulators with multiple links have typically examined only revolute joints **[Yuan,89a]**, analyses of prismatic joints are potentially difficult because the assumed mode method is no longer applicable. However, if the prismatic joint motion bandwidth is below the structural frequencies, the assumed mode method appears to be accurate **[Chalhoub,86 and Yuh,89]**, and the above discussion may still be applicable.

3.4 ISSUE OF COMPOSITE MATERIALS FOR CONSTRUCTION

Composite materials could have two potential roles in the construction of the long-reach manipulators that could significantly improve its performance, stiffness (and strength), and damping. As mentioned previously, for most common materials such as aluminum and steel, the deflections and the natural frequencies are about the same because of the approximately constant factor E/ρ. To increase this factor significantly and therefore the beam stiffness, special composite materials would have to be used; however, a ten-fold improvement in E/ρ will only give roughly a three-fold improvement in the lowest structural natural frequency. Furthermore, the cost required to achieve this ten-fold improvement is high; this makes the use of composite materials prohibitive. However, the issue of using composite materials to increase the beam passive damping might hold some promise and will be examined for potential applications for future manipulators. Because of the experimental nature of this project, conventional materials will probably be chosen; aluminum is the obvious choice because of its high yield strength per weight ratio. Factors such as the corrosiveness and radiation level of the materials in the tank will be taken into account in the design process.

4. ANALYSIS OF WORKSPACE REQUIREMENTS

There are several general workspace requirements to be met by the long-reach manipulator for the Environmental Restoration and Waste Management (ER&WM) Program, which involve volumetric coverage, minimum length, minimum wasted work area, elbow position limitations, and manipulability. The manipulator must be able to fully cover the workspace. It should be as short as possible to improve response by increasing the natural frequency. The minimization of the manipulator workspace outside of the tank will minimize unnecessary manipulator length. All of the links of the manipulator have to remain inside the tank while the end-point covers the workspace. This condition can be guaranteed by assuring that the hand, the shoulder, and the elbow of the manipulator remain inside the tank for all configurations. Singularities in the workspace should be avoided; the robot should be able to move in all directions at all points of the workspace.

Most of the above requirements mainly involve the primary degrees of freedom of the manipulator, i.e., discounting the wrist. The length of the manipulator is impacted by the number of access ports which are used; this is the subject of the next section. However, the design problem actually involves the total manipulator, including its wrist. The following section briefly addresses some of the additional issues requiring further investigation for this application.

4.1. IMPACT OF THE NUMBER OF ACCESS PORTS

The objective of this study is to create a table of relations between the ratio K and the number of ports on the top of the storage tank, where

K = (length of the ER&WM robot) / (radius of the storage tank).

The problem of obtaining the minimum necessary length for each case is best solved geometrically.

Figure 4.1 shows the necessary length of a manipulator for waste tank remediation as a function of the number of access ports on the top of the tank. The length for the manipulator for just one hole is equal to the radius R of the waste storage tank, neglecting the additional length required to avoid the boundary singularity.

Table 4.1, on which Fig. 4.1 is based, gives the ratio between the length of the manipulator and the radius of the tank and indicates the rate of change of manipulator length with number of access ports. It shows the minimum necessary length for the manipulator to reach any point of the storage tank.

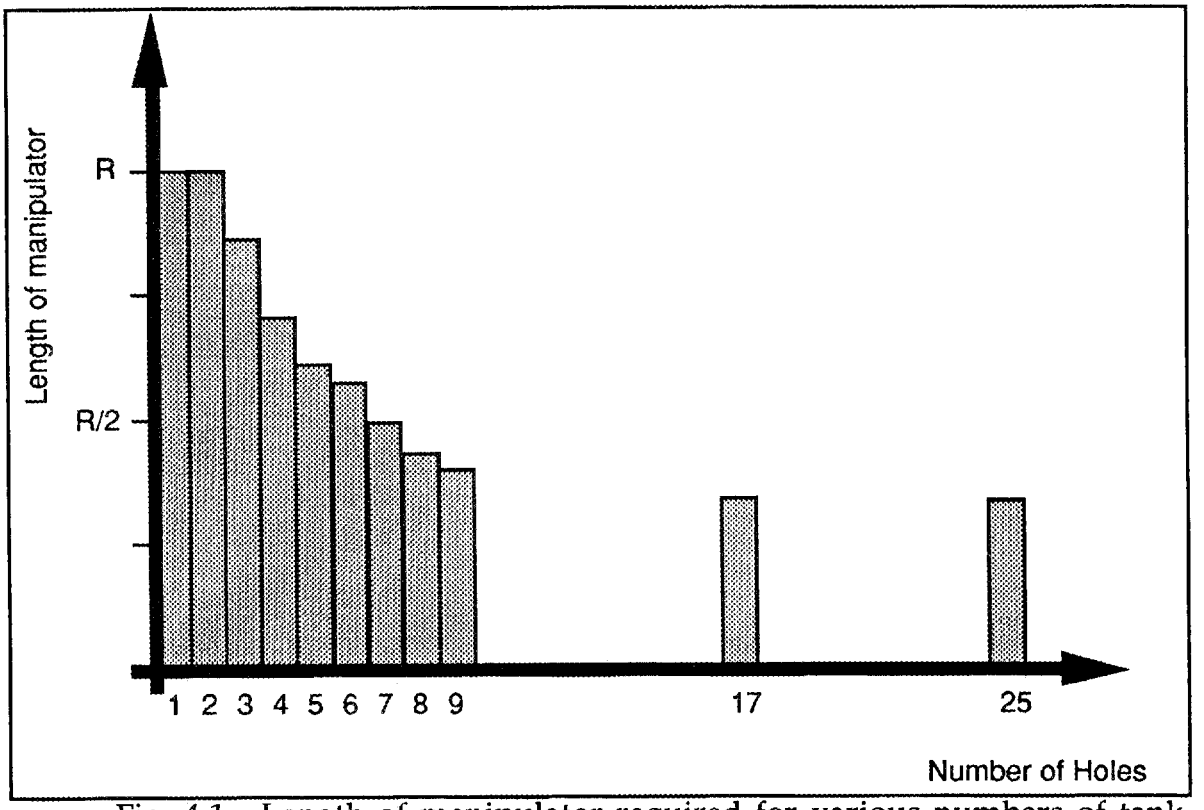

Fig. 4.1. Length of manipulator required for various numbers of tank access ports.

Table 4.1 Rate of change of manipulator length with number of access ports

# of Holes	Length/Radius	Decrease Percentage
1	1	-
2	1	0
3	.866025	13.40
4	.70711	18.35
5	.618034	12.60
6	.57735	6.58
7	.5	13.38
8	.434989	13.00
9	.401388	7.49
17	.346944	1.69
25	.339188	0.28

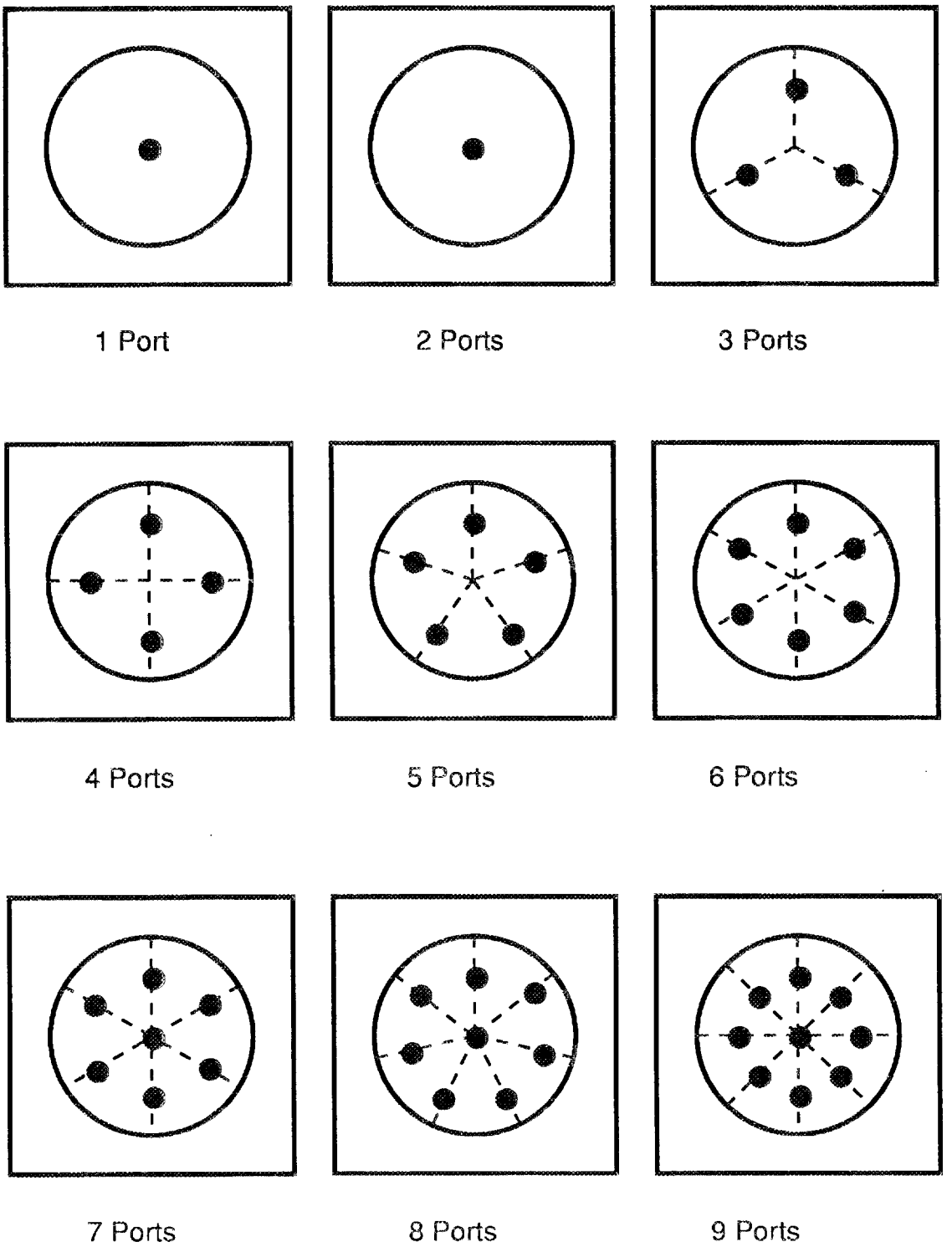

Fig. 4.2. Optimized locations of waste tank ports.

There is no length reduction advantage when having two ports instead of one on the tank. The percentage decrease in the length grows with the increase of the number of ports from two to three and for three to four ports, but it decreases as the number of ports is incremented to five. This indicates that there is more value in going from three to four ports than from four to five.

A good choice of the number of ports will be four. In the event that more ports are needed or can be easily obtained, the next choice should be eight ports. The case of having more ports is not considered here because it will probably be more practical to have the top of the tank removed than to create so many ports.

4.2. OTHER IMPACTS ON THE SELECTION OF A MANIPULATOR KINEMATIC DESIGN FOR WASTE TANK REMEDIATION

In addition to positionally covering the workspace, the design of a manipulator for waste tank remediation should take into account the tasks to be performed which are not clearly defined at this point. One of these tasks may be the positioning of a small, dextrous manipulator to be mounted on the end of the long-reach manipulator. Also, the positioning of a water impulse gun and cutting tools similar to the "jaws of life" used by emergency personnel may be required. Straight-line motions may be required for performing a scooping action, for drilling for samples, or for scabling. More complicated trajectory motions may be required for the use of a circular saw. Those tasks requiring contact will involve force control as well as positioning.

These additional requirements lead one to the selection of a general-purpose manipulator with at least six degrees of freedom and positioning and orienting characteristics which are balanced throughout the workspace.

5. LITERATURE SURVEY ON THE CONTROL OF FLEXIBLE MANIPULATORS AND STRUCTURES

5.1 INTRODUCTION

The control of a flexible manipulator has been and continues to be a very active research area. Basically, three broad categories were observed while conducting a literature survey: (1) open-loop trajectory planning, (2) trajectory following using sensory feedback, and (3) multiple control strategies. Open-loop trajectory planning is basically the problem of determining a suitable actuator command such that the residual vibrations of the trajectory moving in free space are either minimized or eliminated. The planning is done off-line. Trajectory following using sensory feedback is the closed-loop control problem of the manipulator moving in free space. Finally, the multiple control strategies category refers to a combination of different control strategies to handle free-space motion and contact with the environment.

5.2 OPEN-LOOP TRAJECTORY PLANNING

Open-loop trajectory planning can be subdivided into two distinct problems: vibration suppression and inverse dynamic methods. Vibration suppression methods modify the actuator commands so that the resonant frequencies are not excited. Models are fairly simple. The inverse dynamics methods use the full dynamic model of the flexible manipulator and find the actuator command to achieve a desired motion trajectory.

5.2.1 Vibration Suppression

For simple pendulum-type systems, Singhose et al. **[Singhose,90]** proposed an open-loop control scheme by modifying or shaping the command inputs to a flexible system. The residual vibrations were significantly reduced even when significant modeling errors were present making this scheme fairly robust. This method requires very little model information and has been applied to overhead crane-type problems by Noakes et al. **[Noakes,90]**. For off-line applications, acausal filtering was applied by Singer et al. **[Singer,88]** by means of ideal notch filters to remove any undesirable frequency content in a command signal to a flexible manipulator. The manipulator modal frequencies are assumed to be known. Results were applied to a simulator of the space shuttle RMS manipulator with significant reduction in residual vibrations. Mecki et al. **[Mecki,90]** examined shaped inputs constructed from a versine series and applied them to an industrial Cartesian robot. Significant reduction in residual vibrations

were observed. Further, vibrations due to model coupling could also be reduced. A shaped input method to suppress multiple vibrational modes was formulated by Hyde et al. **[Hyde,91]**. Results were applied to linear and nonlinear computer models of a flexible manipulator with fair improvement.

Jones et al. **[Jones,88]** applied an open-loop controller to a gantry system carrying a suspended object. The suspended object was modeled as a simple pendulum. Little residual vibration was observed. Petterson et al. **[Petterson,90]** examined the coupling effect when an accelerated cantilever rod, which sags under gravity, oscillates in both the horizontal and vertical planes. A trajectory planning scheme that could suppress these vibrations was presented. The control algorithm could be easily implemented requiring only modest computational resources. Modeling errors and their effect were also discussed. The results were applied successfully to an actual cantilever rod held by a rigid robot. Christian et al. **[Christian,90]** constructed a three degree-of-freedom flexible manipulator with classical PD servo loops. A non-dimensional analysis was performed based on very simple pendulum type models. Selection of motion trajectories were found which excited little residual vibration in the manipulator.

5.2.2 Inverse Dynamic Methods

Bayo **[Bayo,87a]** presented a method based on a finite-element, frequency-domain formulation of the inverse dynamic problem. The single-link case was addressed. A trajectory based on a Gaussian velocity profile was compared by Bayo et al. **[Bayo,87b]** to the double square pulse acceleration profile used in bang-bang type of control. The Gaussian velocity profile gave very smooth behavior of the flexible single link. An inverse dynamic method based on a frequency-domain formulation was used to arrive at the required actuating torque. To reduce the computational time, Bayo et al. **[Bayo,89]** developed a more efficient algorithm to perform the inverse dynamics of a single line manipulator in real time. An extension to the multi-link case would require parallelization of the algorithms to achieve comparable computational speeds. Kwon et al. **[Kwon,90]** examined the numeric problems associated with the nonminimum phase condition of a flexible structure. The inverse dynamics of a flexible manipulator will contain positive real value poles and anticausal characteristics. Both problems where successfully solved and a joint trajectory was generated given a desired tip trajectory. Results were implemented on a direct drive, single-link flexible manipulator with excellent results. Joint position and velocity were also used to reduce the effects of joint friction and positioning

errors. Serna et al. **[Serna,90]** carried out the inverse dynamic problem in the frequency domain. An optimization problem was formulated to avoid torque limits and bandwidth limitations of the model and the servo system. Computer simulations for a one-link flexible manipulator are presented to show the versatility of the method.

5.3 TRAJECTORY FOLLOWING USING SENSORY FEEDBACK

A discussion of trajectory following using sensory feedback can be subdivided into five areas: (1) nonadaptive control methods, (2) beam redesign and torque transmission relocation, (3) adaptive and robust control, (4) high-performance end-effectors for dynamic compensation, and (5) repetitive control systems.

5.3.1 Nonadaptive Control

Kotnik et al. **[Kotnik,88]** examined various control schemes on a single link flexible manipulator. Basically, two types of feedback sensors were examined: endpoint position sensed by a line-scan camera and an endpoint acceleration sensor. Using the line-scan camera, it was noticed that the observer with full state feedback for pole placement had problems with an observer spillover phenomenon and gave a pronounced steady-state oscillation in comparison with a design based on the root locus method. Using tip acceleration feedback gave good results in comparison with the line-scan camera designs except for large slewing angles commands where a noticeable overshoot was observed.

Book and Majette **[Book,83]** formulated the flexible manipulator problem in the frequency domain and then state variable design methods were applied to arrive at a suitable controller. Since the flexible manipulator is a distributive parameter system, boundary conditions are affected by the controller design and by gain selection. An iterative method was proposed and convergence to a satisfactory design was demonstrated by examples but were not proven.

Cannon and Schmitz **[Cannon,84]** derived an optimal linear feedback signal based on LQR techniques for a linear single-link flexible manipulator. A photodiode arrangement at the tip of the manipulator was used to measure tip position. Hub rate and position sensors were also used. Detail models were required with the inherent limitation of beam performance determined by the wave-propagation delay of the beam. Lee et al. **[Lee,90]** introduce the concept of applying a Jacobian operator to a flexible manipulator. A two-link flexible manipulator was constructed with strain gages attached to the root of each link. Hub position and rates were measured for each joint. Direct

current motors with harmonic drives having ratios of 100:1 and 110:1 were used. The position of the end effector on the horizontal plane was measured by means of a camera system. Stability was addressed for the linear planar case.

Wang et al. **[Wang,89]** implemented a novel sensor using a He-Ne laser with a photodetector to measure the slope of the beam deflection. Further, a shaft encoder was used to measure the hub angle and a single link flexible manipulator was constructed using a dc motor with harmonic drive. The laser measurement system was located at 1% of the beam length from the hub to avoid noncollocation effects. Feeding these control signals back to a simple PD type controller was successful in tracking hub position and compared favorably with simulated results. Tip position tracking was not examined. Sakawa et al. **[Sakawa,85]** constructed a state observer by measuring the strain of the manipulator at the hub. In addition, hub position and velocity were also measured and feedback to the controller. Pole assignment of the controller was accomplished by minimizing a performance criteria. Results were successfully applied to one manipulator.

Schoenwald et al. **[Schoenwald,91]** determined an optimal feedforward trajectory based on a finite-element model of a two-degree-of-freedom (DOF) flexible manipulator. Further, to correct for model errors, feedback gains were calculated based on a quadratic cost criterion. Sensors included two joint position sensors, two joint tachometers, and nine strain gages were placed at each node segment. Results were applied to an actual two DOF flexible manipulator. Performance was very sensitive to model errors. De Maria and Siciliano **[De Maria,87]** formulated the control of a single link flexible arm by means of singular perturbations. A composite control strategy was obtained based on full state availability. Problems associated with full state availability were not discussed. Results were simulated on the computer. Siciliano and Book **[Siciliano,88]** used a singular perturbation strategy to a one DOF flexible beam model and were able to decompose the system dynamics into fast and slow subsystems. A composite controller for both of these subsystems has been designed. The slow subsystem controller is designed similar to computed torque control for rigid manipulators. The fast subsystem controller is designed to stabilize the fast subsystem. Computer simulations were performed indicating feasibility of the method. Vinke and Vidyasagar **[Vinke,91]** applied H_2 optimal control theory to a flexible manipulator while maintaining realistic bounds on the input energy to the actuators. Simulations were performed with application to an actual flexible manipulator still under way.

5.3.2 Beam Redesign and Torque Transmission Relocation

Asada et al. **[Asada,90]** and Park **[Park,90]** were able to change the nonminimum phase control problem associated with the noncollocation problem of a flexible beam by adding either belts or cables at a point remote from the actuators. Further, by modifying the beam geometry, the poles of the beam can be relocated. Simple PD-control can then be applied. A one-link flexible manipulator was constructed to verify the results of the paper. Only planar motions were examined in the paper. Zalucky and Hardt **[Zalucky,84]** constructed a special two parallel beam link with a positional sensor and a hydraulic actuator and servovalve. As the load carrying one beam deflects under the load, the other beam will be used as a base to control the hydraulic actuator to adjust the load-carrying beam. While static deflection correction was the main goal, dynamic correction appears to be possible. The twin-beam was constructed, and significant improvement in beam deflection was observed.

5.3.3 Adaptive and Robust Control

Korolov and Chen **[Korolov,89]** constructed a robust controller with a reduced order observer using tip position sensor, hub rate sensor, and a strain gage sensor almost at the hub. Using a computer simulation of a one-link flexible manipulator, payload masses were varied from 0 to almost 15 times the total mass of the manipulator. Simulated results demonstrated the overall robustness of this controller. Yuan et al. **[Yuan,89a]** applied a model reference adaptive control scheme to a single link flexible manipulator. The control was decomposed into an adaptive control signal and a linear control signal. A state observer was used to estimate all relevant state variables. Strain gages were used to estimate missing states. Although good performance was indicated in simulations, the authors were cautious about extrapolating the results to the multi-link flexible case. Yuh **[Yuh,87]** designed a model-reference adaptive controller based on hyperstability theory and applied the controller to a computer simulation of a one DOF flexible manipulator. Collocated and noncollocated sensors and actuators were examined.

The noncollocated case required significantly larger amounts of actuator power than the collocated case. While a model-reference adaptive controller was effective, further work was needed to evaluate the practical implementation of the noncollocated case. Chen and Menq **[Chen,90]** tested various control schemes on a single flexible manipulator to determine their effectiveness for payload adaptability. Sensors included a tachometer to measure hub rate and a linear incremental encoder to measure tip position. Various identification schemes were tested and combined with a self-tuning controller to ascertain performance. Identification schemes included a

recursive least-squares method, a least-squares method with payload separated, and a modified gradient-based method with averaging scheme. The modified gradient-based method with averaging performed the best against unmodeled dynamic effects and was selected for the self-tuning controller. Feliu et al. **[Feliu,89]** examined changes in payload and the presence of joint friction on a single-link flexible manipulator. Sensors included a potentiometer to provide the hub position and a camera to track the tip position using an infrared sensor. A high-gain inner control loop was designed to reduce the joint friction effects. An outer loop was designed to adapt to changes in payload by tracking the natural frequency of the first wave mode of the manipulator. The control algorithms computational requirement were very modest.

Yurkovich et al. **[Yurkovich,90]** applied a recursive least-squares algorithm to estimate model parameters in conjunction with a one-step-ahead predictor. An adaptive controller was utilized after the joint movement was initiated. A two-link flexible manipulator was constructed with accelerometers mounted on each link. Joint positions and velocities were also measured. Independent joint ARMA model assumptions were made with a discussion of their validity. Using a recursive least-squares algorithm to estimate model parameters in conjunction with a one-step ahead predictor, an adaptive controller was utilized after the joint movement was initiated. The controller was able to adapt to payload changes. Tzes and Yurkovich **[Tzes,90]** applied frequency domain techniques for the implementation of a self-tuning adaptive controller to offset some of the difficulties of time domain estimation methods. This method was applied to a one degree-of-freedom, direct-drive manipulator with collocated shaft rate and position sensors. The controller was able to adapt to payload changes by estimating the first modal frequency and modifying the feedback controller so that the first mode was not excited.

Cetinekunt and Book **[Cetinekunt,90a]** examined inherent performance limitations of a flexible manipulator. Inherent closed-loop bandwidth limitations of two-thirds of the lowest natural frequency of the arm with all joints clamped were reported. An adaptive model following control scheme was also shown to be limited by the structural natural frequencies. Computer simulations on a two-link manipulator were used to verify conclusions. Cetinekunt and Wu **[Cetinekunt,90b]** designed a self-tuning regulator based on predictive adaptive methods. A lattice filter to identify model parameters used only tip position and hub rate measurements. A one-link flexible manipulator was simulated. Robustness issues were deferred to a later study. Based on gradient methods, Nelson and Mitra **[Nelson,86]** estimated the payload mass for a one DOF manipulator and parameterized the optimal feedback gains in terms of the payload mass resulting in little on-line computation. Results were simulated on the computer. A modification of the Massachusetts Institute of Technology (MIT) rule for payload adaptation

control, Menq and Chen **[Menq,88]** designed an adaptive controller using tip position and velocity measurement and hub position and velocity measurement. Results were simulated on the computer for a one-link case.

5.3.4 High-Performance End-effector for Dynamic Compensation

Chiang et al. **[Chiang,91]** examined the situation where a one DOF rigid minimanipulator was attached to a one-link flexible manipulator. End-point sensing was provided by means of a photodiode. Significantly higher bandwidths were achieved by carefully designing the minimanipulator so that the minimum phase condition did not occur. Because of the avoidance of the minimum phase condition, simple lead compensation could be implemented, and the overall controller design was robust to system parameter variations. Dubowsky and Tanner **[Dubowsky,87]** examined a rigid manipulator mounted on a moving vehicle. The results presented are also applicable to a rigid manipulator mounted on a flexible manipulator. The motion of the flexible manipulator can be regarded as a disturbance (assuming the system is stable) and its effect can be compensated. Feedforward compensation using measured base motion of the platform was utilized to improve the trajectory tracking. A PUMA 260 robot on a moving base platform was used to test out the method. The results were encouraging.

5.3.5 Repetitive Control System

The performance of a flexible structure following a repetitive trajectory can be significantly enhanced by means of a technique called repetitive control. The results have been applied successfully to computer disk drive systems for a number of years. The basic idea is presented in Chew and Tomizuka **[Chew,89]** based on the work of Hara et al. **[Hara,88]**.

5.4 MULTIPLE CONTROL STRATEGIES

A possible fourth area of classification is multiple control strategies. Included in this classification are bracing strategies, typically exemplified by a human bracing his wrist when writing, and contact control, in which the control strategy is changed one or more times as contact occurs.

5.4.1 Bracing Strategies

West and Asada **[West,a]** **[West,b]** introduced the bracing concept to a flexible manipulator. Lew and Book **[Lew,90]** examined the use of bracing for large flexible manipulators having high payload capacity but poor positional

and force accuracies. A small manipulator has the opposite attributes. If a large manipulator with high payload capacity is guided by means of a much smaller arm in a braced position, the large manipulator can potentially have the accuracies of the small arm while still maintaining its high payload capacity and workspace volume.

5.4.2 Contact Control

Book and Kwon **[Book,90]** combined an inverse dynamics method to position a flexible manipulator near the contact object and then switched to a force controller to apply the desired level of force without exciting arm vibration. The results were successfully applied to a one DOF direct drive link. Sensory feedback included signals from strain gages located at the base of the link and at its midpoint, joint position, and joint velocity.

6. MODELING OF SINGLE LINK FLEXIBLE STRUCTURES

6.1 A TRANSFER FUNCTION APPROACH

The approach most researchers have taken in arriving at a useful beam model has been typically based on the assumed modes method. Typically, two to three modes are selected (typically clamped-free modes are picked) and state space equations are derived. The weaknesses of this approach are:

1. higher order modes might be significant in some application (ex., observer spillover phenomenon), and
2. forces and moments at the end of the manipulator cannot be easily handled in the modal derivation which are important for our application (i.e., clamped-free modes might not be applicable).

To overcome these limitations, a transfer function approach has been investigated. This approach has been taken by other researchers **[Cetinekunt,91]** and is based on classical Laplace Transform methods **[LePage,61]**.

6.1.1 Model Development

For a single-link flexible manipulator, the governing equations describing the link dynamics are well known, and the following assumptions are typically made:

1. The beam deflections are small compared with the beam length (<0.1L).
2. All terms involving $\dot{\theta}^2$ are negligible.
3. Rotary inertia and shear deformation effects are ignored (i.e, the Euler Bernoulli beam model will be used).

The Euler Bernoulli beam equation is

$$E\,I\,\frac{\partial^4 y(x,t)}{\partial x^4} + \rho\,A\,\frac{\partial^2 y(x,t)}{\partial t^2} = 0 \quad , \tag{6.1}$$

where $0 < x < L$ and the associated boundary conditions are

$$y|_{x=0} = 0 \quad , \tag{6.2a}$$

$$E\,I \left.\frac{\partial^2 y}{\partial x^2}\right|_{x=0} + u = J_h \left[\frac{d^2}{dt^2}\left(\frac{\partial y}{\partial x}\right)\right]_{x=0} , \tag{6.2b}$$

$$E\,I \left.\frac{\partial^2 y}{\partial x^2}\right|_{x=L} = -J_p \left[\frac{d^2}{dt^2}\left(\frac{\partial y}{\partial x}\right)\right]_{x=L} + M(t) , \tag{6.2c}$$

$$F(t) + E\,I \left.\frac{\partial^3 y}{\partial x^3}\right|_{x=L} = m_p \left.\frac{d^2 y}{dt^2}\right|_{x=L} , \tag{6.2d}$$

$$y|_{t=0} = 0 , \tag{6.2e}$$

$$\left.\frac{\partial y}{\partial t}\right|_{t=0} = 0 . \tag{6.2f}$$

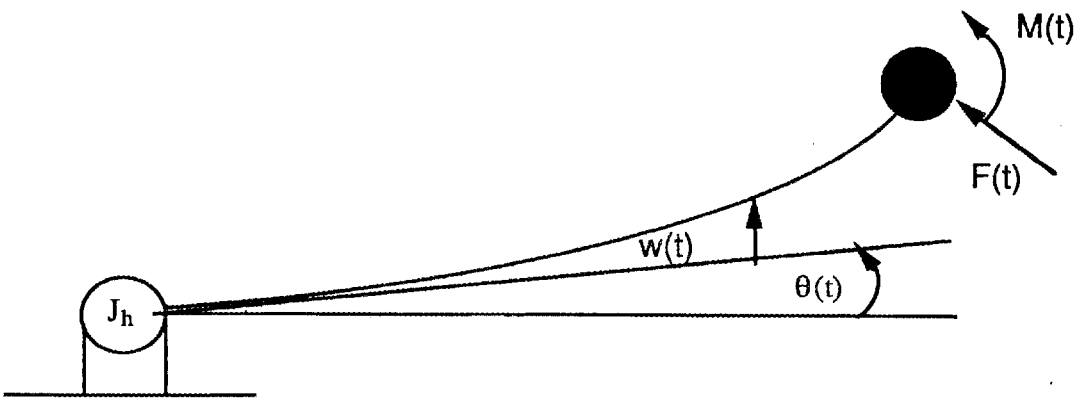

Fig. 6.1. Beam parameters.

To find the beam transfer function, take the Laplace Transform of Eqs. (6.1 - 6.2) where the Laplace Transform of y(x,t) is Y(x,s). These equations transform to the following:

$$\frac{d^4 Y}{d\xi^4} - \beta^4 Y = 0 , \tag{6.3}$$

$$Y|_{x=0} = 0 , \tag{6.4a}$$

$$\left.\frac{d^2 Y}{d\xi^2}\right|_{\xi=0} + U' = -\beta^4 J_h' \left.\frac{dY}{d\xi}\right|_{\xi=0} , \tag{6.4b}$$

$$\left.\frac{d^2Y}{d\xi^2}\right|_{\xi=1} = \beta^4 J_p' \left.\frac{dY}{d\xi}\right|_{\xi=1} + M'(t) \quad , \tag{6.4c}$$

$$\left.\frac{d^3Y}{d\xi^3}\right|_{\xi=1} = -\beta^4 m_p' Y|_{\xi=1} - F'(s) \quad , \tag{6.4d}$$

$$\lim_{s\to\infty} s\,Y = 0 \quad , \tag{6.4e}$$

$$\lim_{s\to\infty} s^2\,Y = 0 \quad , \tag{6.4f}$$

where

$$m_p' = \frac{m_p}{L\,\rho\,A} \quad , \tag{6.5a}$$

$$J_p' = \frac{J_p}{L^3\,\rho\,A} \quad , \tag{6.5b}$$

$$J_h' = \frac{J_h}{L^3\,\rho\,A} \quad , \tag{6.5c}$$

$$\beta^4 = -\,s^2\,\frac{\rho\,A\,L^4}{E\,I} \quad , \tag{6.5d}$$

$$M' = \frac{M\,L^2}{E\,I} \quad , \tag{6.5e}$$

$$F' = \frac{F\,L^3}{E\,I} \quad , \tag{6.5f}$$

$$\xi = \frac{x}{L} \quad . \tag{6.5g}$$

$Y(\xi,s)$ can be written in the following convenient form

$$Y(\xi,s) = A(s)\sin\beta\,\xi + B(s)\sinh\beta\,\xi + C(s)\cos\beta\xi + D(s)\cosh\beta\,\xi \tag{6.6}$$

with the problem of the selecting suitable values for A, B, C, and D based on the boundary conditions specified by Eqs. (6.4a - 6.4f). Equation (6.4a) constrains Eq. (6.6) such that

$$D(s) = -\,C(s) \tag{6.7}$$

A, B, and C can be solved by inserting Eq. (6.6) into the boundary conditions given by Eq. (6.4b-6.4d) and casting into a matrix form like

$$N\begin{bmatrix} A \\ B \\ C \end{bmatrix} = \begin{bmatrix} -M' \\ -F' \\ -U' \end{bmatrix} , \tag{6.8}$$

where $N = [n_{ij}]$ with each term defined as

$$n_{11} = \beta^2\left(\beta^3 J_p' \cos\beta + \sin\beta \right) , \tag{6.9a}$$

$$n_{12} = \beta^2\left(\beta^3 J_p' \cosh\beta - \sinh\beta \right) , \tag{6.9b}$$

$$n_{13} = -\beta^5 J_p' \left(\sinh\beta + \sin\beta\right) + \beta^2\left(\cosh\beta + \cos\beta\right) , \tag{6.9c}$$

$$n_{21} = \beta^3\left(\beta m_p' \sin\beta - \cos\beta \right) , \tag{6.9d}$$

$$n_{22} = \beta^3\left(\beta m_p' \sinh\beta + \cosh\beta \right) , \tag{6.9e}$$

$$n_{23} = \beta^4 m_p' \left(\cos\beta - \cosh\beta\right) + \beta^3\left(\sin\beta - \sinh\beta\right) , \tag{6.9f}$$

$$n_{31} = \beta^5 J_h' , \tag{6.9g}$$

$$n_{32} = \beta^5 J_h' \text{ , and} \tag{6.9h}$$

$$n_{33} = -2\,\beta^5 . \tag{6.9i}$$

The solution becomes simply

$$Y(\xi,s) = \begin{bmatrix} \sin\beta\xi \\ \sinh\beta\xi \\ \cos\beta\xi - \cosh\beta\xi \end{bmatrix}^T N^{-1} \begin{bmatrix} -M' \\ -F' \\ -U' \end{bmatrix} , \tag{6.10}$$

which can be rewritten as

$$Y(\xi,s) = H_m^y M' + H_f^y F' + H_u^y U' , \tag{6.11}$$

where H_m^y, H_f^y, and H_u^y are transfer functions defined as

$$H_m^y = \left.\frac{Y}{M'}\right|_{F'=0;U'=0} , \tag{6.12a}$$

$$H_f^y = \left.\frac{Y}{M'}\right|_{M'=0;U'=0} , \tag{6.12b}$$

$$H_u^y = \left.\frac{Y}{M'}\right|_{M'=0;F'=0} . \tag{6.12c}$$

The hub angle can be determined from Eq. (6.10) using the fact that

$$\theta(s) = \frac{1}{L}\left.\frac{\partial Y(\xi,s)}{\partial \xi}\right|_{\xi=0} = \frac{\beta}{L}\begin{bmatrix} 1 \\ 1 \\ 0 \end{bmatrix}^T N^{-1}\begin{bmatrix} -M' \\ -F' \\ -U' \end{bmatrix} , \tag{6.13a}$$

which can be rewritten in a normalized fashion as

$$\theta'(s) = L\,\theta(s) = \left.\frac{\partial Y(\xi,s)}{\partial \xi}\right|_{\xi=0} = \beta\begin{bmatrix} 1 \\ 1 \\ 0 \end{bmatrix}^T N^{-1}\begin{bmatrix} -M' \\ -F' \\ -U' \end{bmatrix} . \tag{6.13b}$$

Similarly, the hub transfer functions are

$$\theta(s) = H_m^\theta M' + H_f^\theta F' + H_u^\theta U' , \tag{6.14}$$

where H_m^θ, H_f^θ, and H_u^θ are transfer functions defined as

$$H_m^\theta = \left.\frac{\theta}{M'}\right|_{F'=0;U'=0} , \tag{6.15a}$$

$$H_f^\theta = \left.\frac{\theta}{M'}\right|_{M'=0;U'=0} , \tag{6.15b}$$

$$H_u^\theta = \left.\frac{\theta}{M'}\right|_{M'=0;F'=0} . \tag{6.15c}$$

Moments along the beam can be measured by means of strain gages and can be modeled in a similar manner as above by noting that

$$m(\xi,s) = \frac{E\,I}{L^2}\frac{\partial^2 Y(\xi,s)}{\partial \xi^2} = \beta^2\frac{E\,I}{L^2}\begin{bmatrix} -\sin\beta\,\xi \\ \sinh\beta\,\xi \\ -\cos\beta\,\xi - \cosh\beta\,\xi \end{bmatrix}^T N^{-1}\begin{bmatrix} -M' \\ -F' \\ -U' \end{bmatrix} , \tag{6.16a}$$

which can be rewritten in a normalized fashion as

$$m'(\xi,s) = \frac{L^2}{EI} m(\xi,s) = \frac{\partial^2 Y(\xi,s)}{\partial \xi^2} = \beta^2 \begin{bmatrix} -\sin \beta \xi \\ \sinh \beta \xi \\ -\cos \beta \xi - \cosh \beta \xi \end{bmatrix}^T N^{-1} \begin{bmatrix} -M' \\ -F' \\ -U' \end{bmatrix} . \quad (6.16b)$$

Similarly, the moment transfer functions are

$$m'(\xi,s) = H_m^m M' + H_f^m F' + H_u^m U' , \quad (6.17)$$

where H_m^m, H_f^m, and H_u^m are transfer functions defined as

$$H_m^m = \left.\frac{m}{M'}\right|_{F'=0;U'=0} , \quad (6.18a)$$

$$H_f^m = \left.\frac{m}{M'}\right|_{M'=0;U'=0} , \quad (6.18b)$$

$$H_u^m = \left.\frac{m}{M'}\right|_{M'=0;F'=0} . \quad (6.18c)$$

One final normalization is needed to make the simulations and controller independent of the beam parameters. Since $\beta^4 = -s^2 \frac{\rho A L^4}{EI}$, replace s with a normalized s, $\hat{s}$,

$$\hat{s} = \frac{s}{\frac{1}{L^2}\sqrt{\frac{EI}{\rho A}}} . \quad (6.19)$$

All of the transfer functions will be, unless otherwise written, in terms of $\hat{s}$ and ξ (both complex frequency and beam location have been normalized) with the cap on the normalized frequency dropped for convenience.

6.1.2 Product Expansions for Transfer Function Models

6.1.2.1 Analytic and Numeric Issues

The transfer functions introduced in the previous section are different from those encountered in ordinary differential models. Ordinary differential models will have transfer functions that can be represented as a product expansion with a finite number of products. However, the transfer function for a flexible manipulator is more complex, as the reader can observe from Eqs. (6.10, 6.13, and 6.16).

Based on the Mittag-Leffler theorem **[Lee,90]**, the transfer function for a flexible manipulator will have an infinite product expansion of separable factors. A concise summary of infinite product expansions for distributed systems is given by Goodson **[Goodson,70]**. For practical modeling and simulations, the product expansion for the transfer function will be truncated at a certain number of terms which is similar to the assumed modes method of only including the first two or three modes.

To solve for the roots of flexible manipulator transfer function can be simplified by the following theorems:

Theorem 1: The poles for the above transfer function will lie only on the $j\omega$ axis in the s-plane or on either the real or the imaginary axis in the β-plane.

Theorem 2: The zeros for the above transfer function will lie either on the real or the imaginary axis in the s-plane. Roots on the imaginary axis of the s-plane will map to roots on either the real or the imaginary axis in the β-plane. Roots on the real axis of the s-plane will map to line segments in the β-plane passing through the origin to points (1+ j), (1 - j), (-1 + j), and (-1 - j). Proofs for the above two theorems are given by Spector **[Spector,90]**.

Muller's method **[Press,86]**–which is typically used to solve for the roots of an analytical function, F(s), such as those presented in this paper–was used. Implementation of Muller's method can be easily performed and appears to be fairly robust. Explicit computer code is given in **[Press,86]**. The roots were scanned in the β-plane exploiting the restriction that the roots can only lie on a certain line based on the above two theorems.

The order, n, of the roots (i.e., multiplicity of roots) was determined by a simple scan around a root, s_0, and calculating the change in the function, F(s).

$$n = \frac{\ln F(s_1) - \ln F(s_2)}{\ln 2}, \tag{6.20}$$

where

$s_1 = \varepsilon + s_0$,

$s_2 = 2\varepsilon + s_0$,

ε = small real number (around 1e-3 to 1e-2 worked well).

Likewise, to determine the dc-gain constant, K_{dc},

$$K_{dc} = \frac{-\ln F(s_1) \ln s_2 - \ln F(s_2) s_1}{\ln 2}, \tag{6.21}$$

where $s_0 = 0$.

6.1.2.2 Listing of Normalized Transfer Function

In this section, a listing of the roots, root order, and dc-gain for the normalized transfer function will be given. The listings will cover the range from 0 to 1000 on the imaginary axis and 0 to 1000 on the real axis. The poles for each of the transfer function are provided by the determent of the N matrix and are summarized in Table 6.1.

Table 6.1. Pole locations for all transforms

Normalized roots	Multiplicity
0 + j 0	5
0 ± j 15.4182	1
0 ± j 49.9649	1
0 ± j 104.2477	1
0 ± j 178.2697	1
0 ± j 272.0310	1
0 ± j 385.5314	1
0 ± j 518.7711	1
0 ± j 671.7499	1
0 ± j 844.4680	1

Table 6.2a. $H_{\hat{u}}^{y}$ zero locations ($\xi = 1$ and $K_{dc} = 1$)

Normalized roots	Multiplicity
0 + j 0	3
± 11.1866 + j 0	1
± 60.4517 + j 0	1
± 149.2778 + j0	1
± 277.5826 + j 0	1
± 445.3659 + j 0	1
± 652.6314 + j 0	1

Table 6.2b. H_0^y zero locations ($\xi = 0.9$ and $K_{dc} = 1$)

Normalized roots	Multiplicity
$0 + j\,0$	3
$\pm\ 14.8131 + j\,0$	1
$\pm\ 87.9097 + j\,0$	1
$\pm\ 216.4080 + j\,0$	1
$\pm\ 389.6888 + j\,0$	1
$\pm\ 609.0982 + j\,0$	1
$\pm\ 879.6370 + j\,0$	1
$0 \pm j\,107.8269$	

Table 6.2c. H_0^y zero location ($\xi = 0.8$ and $K_{dc} = 1$)

Normalized roots	Multiplicity
$0 + j\,0$	3
$\pm\ 25.9575 + j\,0$	1
$\pm\ 123.3701 + j\,0$	1
$\pm\ 277.0631 + j\,0$	1
$\pm\ 493.1869 + j\,0$	1
$\pm\ 771.0247 + j\,0$	1
$0 \pm j\,25.9672$	1
$0 \pm j\,382.7618$	1

Table 6.2d. H_u^y zero location ($\xi = 0.7$ and $K_{dc} = 1$)

Normalized roots	Multiplicity
0 + j 0	3
± 40,1139 + j 0	1
± 160.7569 + j 0	1
± 362.5383 + j 0	1
± 644.5439 + j 0	1
± 1007.1023 + j 0	1
0 ± j 12.7697	1
0 ± j 170.1192	1
0 ± j 555.2598	1

Table 6.2e. H_u^y zero location ($\xi = 0.6$ and $K_{dc} = 1$)

Normalized roots	Multiplicity
0 + j 0	3
± 54.5764 + j 0	1
± 219.3165 + j 0	1
± 493.4795 + j 0	1
± 877.2982 + j 0	1
0 ± j 8.9468	1
0 ± j 95.6335	1
0 ± j 312.3316	1
0 ± j 651.5448	1

Table 6.2f. H_u^y zero location ($\xi = 0.5$ and $K_{dc} = 1$)

Normalized roots	Multiplicity
$0 + j\,0$	1
$\pm 78.7685 + j\,0$	1
$\pm 315.8266 + j\,0$	1
$\pm 710.6115 + j\,0$	1
$0 \pm j\,7.03912$	1
$0 \pm j\,60.8261$	1
$0 \pm j\,199.9276$	1
$0 \pm j\,416.9865$	1
$0 \pm j\,713.0791$	1

Table 6.2g. H_u^y zero location ($\xi = 0.4$ and $K_{dc} = 1$)

Normalized roots	Multiplicity
$0 + j\,0$	3
$0 \pm j\,5.8469$	1
$0 \pm j\,43.2609$	1
$0 \pm j\,138.4602$	1
$0 \pm j\,289.6069$	1
$0 \pm j\,495.1988$	1
$0 \pm j\,755.6400$	1
$\pm 123.3701 + j\,0$	1
$\pm 493.4802 + j\,0$	1

Table 6.2h. H_0^y zero location ($\xi = 0.3$ and $K_{dc} = 1$)

Normalized roots	Multiplicity
$0 \pm j\,0$	3
$0 \pm j\,5.0134$	1
$0 \pm j\,33.9198$	1
$0 \pm j\,102.1313$	1
$0 \pm j\,212.2553$	1
$0 \pm j\,363.7205$	1
$0 \pm j\,555.2058$	1
$0 \pm j\,786.8138$	1
$\pm 219.3245 + j\,0$	1
$\pm 877.29812 + j\,0$	1

Table 6.2i. H_0^y zero location ($\xi = 0.2$ and $K_{dc} = 1$)

Normalized roots	Multiplicity
$0 + j\,0$	3
$0 \pm j\,4.3910$	1
$0 \pm j\,28.3255$	1
$0 \pm j\,81.4961$	1
$0 \pm j\,164.1530$	1
$0 \pm j\,278.2691$	1
$0 \pm j\,424.3603$	1
$0 \pm j\,601.9471$	1
$0 \pm j\,810.4462$	1
$0 \pm j\,1049.6337$	1
$\pm\ 493.4802 + j\,0$	1

Table 6.2j. H_u^y zero location ($\xi = 0.1$ and $K_{dc} = 1$)

Normalized roots	Multiplicity
$0 + j\,0$	3
$0 \pm j\,3.9058$	1
$0 \pm j\,24.6328$	1
$0 \pm j\,69.3716$	1
$0 \pm j\,136.7519$	1
$0 \pm j\,227.4116$	1
$0 \pm j\,341.7365$	1
$0 \pm j\,480.1045$	1
$0 \pm j\,642.8422$	1
$0 \pm j\,830.1969$	1
$0 \pm j\,1042.3158$	

Table 6.3. H_f^y zero location ($\xi = 1$ and $K_{dc} = 1$)

Normalized roots	Multiplicity
$0 + j\,0$	3
$0 \pm j\,9.8696$	1
$0 \pm j\,39.4784$	1
$0 \pm j\,88.8264$	1
$0 \pm j\,157.9137$	1
$0 \pm j\,246.7401$	1
$0 \pm j\,355.3058$	1
$0 \pm j\,483.6106$	1
$0 \pm j\,631.6547$	1
$0 \pm j\,799.4380$	1
$0 \pm j\,986.9604$	1

Table 6.4. H^{v}_{m} zero location ($\xi = 1$ and $K_{dc} = 1$)

Normalized roots	Multiplicity
$0 + j0$	3
$0 \pm j5.5933$	1
$0 \pm j30.2258$	1
$0 \pm j74.6389$	1
$0 \pm j138.7913$	1
$0 \pm j222.6829$	1
$0 \pm j449.6839$	1
$0 \pm j326.3138$	1
$0 \pm j592.7931$	1
$0 \pm j755.6416$	1
$0 \pm j938.2292$	1

Table 6.5. H^{m}_{u} zero location ($\xi = 0.5$ and $K_{dc} = 1$)

Normalized roots	Multiplicity
$0 + j0$	3
$0 \pm j62.5745$	1
$0 \pm j199.7914$	1
$0 \pm j416.9950$	1
$\pm 21.7568 + j0$	1
$\pm 177.6650 + j0$	1
$\pm 493.4803 + j0$	1
$\pm 967.2212 + j0$	1

Table 6.6. H_u^θ zero location ($\xi = 0$ and $K_{dc} = 1$)

Normalized roots	Multiplicity
$0 + j0$	3
$0 \pm j3.5160$	1
$0 \pm j22.0345$	1
$0 \pm j61.6972$	1
$0 \pm j120.9020$	1
$0 \pm j199.8595$	1
$0 \pm j298.5555$	1
$0 \pm j416.9908$	1
$0 \pm j555.1652$	1
$0 \pm j713.0789$	1
$0 \pm j890.7318$	1

6.1.2.3 Explicit Transfer Function

The basic form for each of the transfer functions are given in this section. The basic issue is that the numerator and the denominator cannot be arbitrarily truncated. To clarify these issues, let us first examine H_u^y. From Tables 6.1 and 6.2a-j, the poles and zeros and be cast in the following form:

$$H_u^y = \frac{K_{dc} \prod_{i=1}^{n} \left[\frac{s^2}{\omega_{zi}^2} + \frac{2\,\delta_{zi}\,s}{\omega_{zi}} + 1 \right]}{s^2 \prod_{j=1}^{d} \left[\frac{s^2}{\omega_{pj}^2} + \frac{2\,\delta_{pj}\,s}{\omega_{pj}} + 1 \right]}, \tag{6.22}$$

where n and d are the order of the numerator and denominator, respectively. If the input is a step function and utilizing Eq. (6.4f), d must be greater than or equal to n. It is interesting to note that modal methods have d equal to n. Based on the simulation methods discussed below, we will set d equal to n. For d equal to n, the transfer function represented by Eq. (6.22) has two zeros at infinity.

Based on Eq. (6.4f) and convenience in the simulation, H_m^y and H_f^y will have the same form as Eq. (6.22) with d equal to n. Also, Eq. (6.22) still holds for H_m^θ, H_f^θ, and H_u^θ.

H_m^m, H_f^m, and H_u^m have the following form:

$$H_u^m = K_{dc} \frac{\prod_{i=1}^{n} \left[\frac{s^2}{\omega_{zi}^2} + \frac{2\,\delta_{zi}\,s}{\omega_{zi}} + 1 \right]}{\prod_{j=1}^{d} \left[\frac{s^2}{\omega_{pj}^2} + \frac{2\,\delta_{pj}\,s}{\omega_{pj}} + 1 \right]} \quad . \tag{6.23}$$

6.1.3 Simulation Method

For a given input, simulation based on a product expansion transfer function is straightforward. Since the transfer functions being addressed in this report are of infinite order, truncation of the transfer function is necessary. It has been observed that truncation of an infinite order product expansion has the property of preserving the extreme values of known, exact solutions (see Goodson **[Goodson,70]** for details). Further, increasing the order of the transfer function is straightforward and provides a straightforward check of the effect of ignoring higher order dynamic terms.

For an arbitrary product expansion H, let Y and U be the Laplace Transforms of the output variable y and input variable u. Describe the product expansion as

$$\frac{Y(s)}{U(s)} = H(s) = \prod_{i=1}^{n} P_i(s) \quad . \tag{6.24}$$

Define $Y_i \equiv P_i\, Y_{i-1}$ and $Y_0 \equiv U$. Then by direct substitution $Y = Y_n$. For a digital simulation, cascading the product terms by means of digital filters (see Fig. 6.2) can be readily accomplished especially since there is only one basic type of filter required.

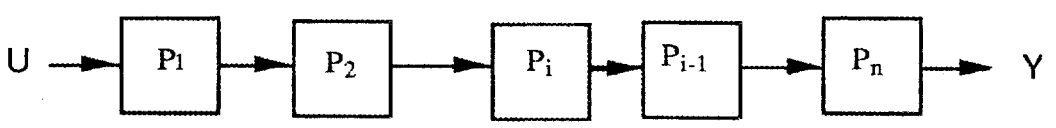

Fig. 6.2. Cascading of filter for simulation of product expansion.

Let

$$P_i = \frac{\dfrac{s^2}{\omega_{zi}^2} + \dfrac{2\,\delta_{zi}\,s}{\omega_{zi}} + 1}{\dfrac{s^2}{\omega_{pi}^2} + \dfrac{2\,\delta_{pi}\,s}{\omega_{pi}} + 1} \quad . \tag{6.25}$$

After converting Eq. (6.23) into the z-domain by means of Tustin bilinear transform $s = \frac{2}{T_s}\frac{z-1}{z+1}$ and after some manipulation, the conversion is

$$P_i(z) = K_i \frac{(1 + \sigma_{1i}\, z^{-1} + \sigma_{2i}\, z^{-2})}{(1 - \alpha_{1i}\, z^{-1} - \alpha_{2i}\, z^{-2})} \quad , \tag{6.26}$$

where

$$K_i = \frac{\Delta_\sigma}{\Delta_\alpha} \quad , \tag{6.27a}$$

$$\Delta_\sigma = 4\, a_{ni} + 2\, b_{ni}\, T_s + T_s^2 \quad , \tag{6.27b}$$

$$\Delta_\alpha = 4\, a_{di} + 2\, b_{di}\, T_s + T_s^2 \quad , \tag{6.27c}$$

$$\sigma_{1i} = \frac{-8\, a_{ni} + 2\, T_s^2}{\Delta_\sigma} \quad , \tag{6.27d}$$

$$\sigma_{2i} = \frac{4\, a_{ni} - 2\, b_{ni} + T_s^2}{\Delta_\sigma} \quad , \tag{6.27e}$$

$$\alpha_{1i} = \frac{8\, a_{di} - 2\, T_s^2}{\Delta_\alpha} \quad , \tag{6.27f}$$

$$\alpha_{2i} = \frac{-4\, a_{di} + 2\, b_{di} - T_s^2}{\Delta_\alpha} \quad , \tag{6.27g}$$

$$a_{di} = \frac{1}{\omega_{pi}^2} \quad , \tag{6.27h}$$

$$a_{ni} = \frac{1}{\omega_{zi}^2} \quad , \tag{6.27i}$$

$$b_{di} = \frac{2\,\delta_{pi}}{\omega_{pi}} \quad , \tag{6.27j}$$

$$b_{ni} = \frac{2\,\delta_{zi}}{\omega_{zi}} \quad . \tag{6.27k}$$

6.2 MODELING OF A FLEXIBLE MANIPULATOR USING MODAL ANALYSIS

In this section, a model of a single link flexible manipulator is derived using the assumed mode method. To derive equations of motion of the manipulator, the position of a point on the beam is described with virtual rigid-body motion and flexible deflection using a Bernoulli-Euler beam model. The virtual rigid-body motion is represented by the motion of the moving rigid coordinate which is attached to the beam. The rigid coordinate can be defined in several ways **[Kwon,90]**. It can be attached at the base hub (clamp-free), it can pass through the center of mass of the beam (pin-free), or it can pass through the end-point (pin-pin). For each definition of the rigid coordinate, different boundary conditions should be used for the flexible mode shape functions. The flexible deflection is represented by a finite series of assumed modes with respect to the moving reference coordinate. In this section, the rigid coordinate that passes through the end point was used because it gives a simple representation of the end-point position.

Using Lagrange's equations of motion, the dynamic equation of a flexible manipulator is obtained with generalized coordinates.

$$\frac{d}{dt}\left(\frac{\partial T}{\partial \dot{q}_i}\right) - \frac{\partial T}{\partial q_i} + \frac{\partial V}{\partial q_i} + \frac{\partial F}{\partial \dot{q}_i} = Q_i \qquad i = 0,1,\cdots,n$$

where T = kinetic energy, V = potential energy, F = dissipation energy by damping, and Q = a generalized force.

$$[M]\,\ddot{q} + [D]\,\dot{q} + [K]\,q = [B]\,\tau \quad .$$

The mass, stiffness, damping, and input matrices are described with mode shape functions in the following general form. They are valid for different definitions of rigid coordinates. The damping matrix represents the joint friction modeled as viscous friction with the coefficient C_0.

$$\text{for } i,j=0,1,\cdots,n \qquad q=\begin{Bmatrix} q_i \\ \vdots \end{Bmatrix}$$

$$[M] = \begin{bmatrix} M_{ij} & \cdots \\ \vdots & \ddots \end{bmatrix}, \quad M_{ij} = \begin{pmatrix} \rho A\int_0^1 \phi_i(x)\phi_j(x)dx \\ +I_h\phi_i'(0)\phi_j'(0) \\ +M_e\phi_i(l)\phi_j(l) \\ +J_e\phi_i'(l)\phi_j'(l) \end{pmatrix}.$$

$$[D] = C_0\begin{bmatrix} \phi_i'(0)\phi_j'(0) & \cdots \\ \vdots & \ddots \end{bmatrix}, \qquad [B] = \begin{bmatrix} \phi_i'(0) \\ \vdots \end{bmatrix}.$$

$$[K] = \begin{bmatrix} 0 & 0 & \cdots \\ 0 & K_{ij} & \cdots \\ \vdots & \vdots & \ddots \end{bmatrix}, \qquad K_{ij} = EI\int_0^1 \phi_i''(x)\phi_j''(x)dx.$$

The dynamic equation can be written as follows in a state space form.

$$\dot{X} = \begin{bmatrix} 0 & I \\ M^{-1}K & M^{-1}D \end{bmatrix} X + \begin{bmatrix} 0 \\ M^{-1}B \end{bmatrix}\tau = [A]\ X + [B^*]\tau$$
$$Y = [C]\,X \qquad \text{where} \quad X = \{q_0, q_1, \cdots, \dot{q}_0, \dot{q}_1, \cdots\}^t.$$

6.3 COMPARISON OF EXACT MODEL WITH MODAL-BASED MODEL

From the system matrices [A], [B*], and [C], the poles and zeros have been calculated and are compared with those from the the exact model using the data of a single-link, long-reach manipulator ($EI = 2.7*10^{10}$ lb_f-in.^{2}, $\rho A = 1.55*10^{-2}$ lb_f-s^2/in.^{2}, L = 360 in.). These comparisons are given in Tables 6.7 and 6.8.

Table 6.7. A comparison of poles for joint torque input and end-point position output

Exact model		Assumed mode model	
Normalized poles	Actual poles (rad/s)	Poles (rad/s) with 2 modes	Poles (rad/s) with 5 modes
j 0 (2 poles)	j 0 (2 poles)	j 0 (2 poles)	j 0 (2 poles)
± j 15.4182	± j 156.8157	± j 157.0897	± j 156.8220
± j 49.9649	± j 508.1777	± j 523.6319	± j 508.3851
± j 104.2477	± j 1060.2875		± j 1062.2353
± j 178.2697	± j 1813.1388		± j 1825.2025
± j 272.0310	± j 2766.7378		± j 2859.7918

The modal-based model is using five pinned-pinned assumed mode shape functions. The comparison table shows that the poles of the modal-based model converges to those of the exact model very well.

Table 6.8. A comparison of zeros for joint torque input and end-point position output

Exact model		Assumed mode model	
Normalized zeros	Actual zeros (1/s)	Zeros (1/s) with 2 modes	Zeros (1/s) with 5 modes
± 11.1866	± 113.7759	± 117.7720	± 113.5811
± 60.4517	± 614.8348	± 342.2325	± 665.892 + j 183.073
± 277.5826	± 2823.2237		± 665.892 - j 183.073
± 445.3659	± 4529.6739		± 933.681 + j 1355.471
± 652.6314	± 6637.5570		± 933.681 - j 1355.471

The exact model shows only real value zeros. These positive real value zeros can be explained with causal and anticausal concepts in the inverse dynamics **[Kwon,91]**. The modal-based model with two modes shows two real value zeros and the first one converges to the exact model's one. However, if more higher modes are included in the model, from third mode on, complex number zeros are obtained. Some researchers have also presented complex value zeros in the modeling of a flexible manipulator **[Cannon,84]**. The interesting issues arise in the physical meaning of the complex zeros and their cause. It could be numerical errors in calculating the system matrix from the mode shape functions, or it could be basic characteristics of the modal-based model. The zero characteristics of a flexible manipulator are currently being investigated further.

7. OPEN-LOOP TRAJECTORY PLANNING

7.1 BASIC APPROACHES

As discussed earlier, open-loop trajectory planning can be subdivided into two distinct approaches: vibration suppression and inverse dynamic methods. Vibration suppression approaches modify the actuator commands so that the resonant frequencies are not excited. Models are fairly simple, and the idea is akin to using a notch filter. The inverse dynamic approach uses the full dynamic model of the flexible manipulator to find the actuator command to achieve a desired motion trajectory. The inverse dynamic problem will be cast into a form that will have poles in the right-half plane (RHP). Poles in the RHP creates a real difficulty in computing actuator torque that will not cause saturation of the drive. Fortunately, the solution is straightforward to correct if one loosens the causality constraint imposed upon the problem. If one allows the actuating torque to start before the starting time of the tip position, then bounded torques exist. This idea is not new; the basic idea was first proposed by Singer et al. **[Singer,88]** by using "ideal" notch filters based on an acausal filtering methods. Kwon **[Kwon,91]** presented a rigorous solution to the problem, and his method is basically the one presented in this report since it also provides insight into the vibration suppression approach. The only extension to Kwon's work is its application to a specific class of trajectories which greatly simplifies the amount of computation required.

7.2 INVERSE DYNAMICS METHOD

The basic object in the inverse dynamic method is to find an input that will drive the flexible link in such a manner that it follows a prescribed trajectory. No contact with the environment is assumed. Since the tip position is related to the actuator by means of the H_u^y, the inverse problem is to find the required actuator torque for a given tip trajectory, i.e.,

$$U(s) = (H_u^y)^{-1}\, Y(s) \quad , \tag{7.1a}$$

or

$$U(s) = \frac{(H_u^y)^{-1}}{s^3}\, J(s) \quad , \tag{7.1b}$$

where $J(s) = s^2 \dot{Y}(s)$ which means that $j(t) = \mathcal{L}^{-1}\{J(s)\}$ is the jerk of the tip. The $\mathcal{L}$ operator is the one-sided Laplace transform and $\mathcal{L}^{-1}$ is its inverse.

The reason for casting the problem as shown in Eq. (6.1b) is that the order of the denominator is one greater than the numerator for $\frac{(H_0^y)^{-1}}{s^3}$ which means that the inverse of this transform exists and one does not have to resort to impulse function representation. For brevity, define

$$T(s) \equiv \frac{(H_0^y)^{-1}}{s^3} = \frac{K_{dc}^{-1}}{s} \frac{\prod_{j=1}^{d}\left[\frac{s^2}{\omega_{pj}^2} + \frac{2\,\delta_{pj}\,s}{\omega_{pj}} + 1\right]}{\prod_{i=1}^{n}\left[\frac{s^2}{\omega_{zi}^2} + \frac{2\,\delta_{zi}\,s}{\omega_{zi}} + 1\right]} , \tag{7.2}$$

where the notation from the last section has been used and n = d is assumed.

The denominator of T(s) will have poles in the right-half plane (RHP) as can be seen from Table 7.2a. To avoid actuator saturation, the causality constraint will be relinquished. This is accomplished by using the two-sided Laplace Transform, $\mathcal{L}_2$ instead of the one-sided Laplace Transform which has been used up to now.

To demonstrate how this method works, Eq. (7.2) will be rewritten since all of the zeros of H_0^y are on the real axis and are symmetrical with respect to the imaginary axis in the s-plane.

$$T(s) = \frac{K_{dc}^{-1}}{s} \frac{\prod_{j=1}^{d}\left[\frac{s^2}{\omega_{pj}^2} + \frac{2\,\delta_{pj}\,s}{\omega_{pj}} + 1\right]}{\prod_{i=1}^{d}\left[\left(\frac{s}{z_i} + 1\right)\left(\frac{s}{-z_i} + 1\right)\right]} , \tag{7.3a}$$

or

$$T(s) = \frac{K_{dc}^{-1}}{s} T_L \; T_R \quad , \tag{7.3b}$$

where $z_i > 0$ and

$$T_L(s) = \prod_{i=1}^{d} \frac{\left(\frac{s^2}{\omega_{pi}^2} + \frac{2\,\delta_{pi}\,s}{\omega_{pi}} + 1\right)}{\left(\frac{s}{z_i} + 1\right)^2} = \frac{N_L(s)}{\prod_{i=1}^{d}\left(\frac{s}{z_i} + 1\right)^2} \quad , \tag{7.3c}$$

$$T_R(s) = \prod_{j=1}^{d} \frac{\left(\frac{s}{z_j} + 1\right)}{\left(\frac{s}{-z_j} + 1\right)} \quad . \tag{7.3d}$$

The L subscript in $T_L(s)$ denotes the transform which has only zeros in the left-half plane (LHP), and the R subscript in $T_R(s)$ denotes the transform which has only zeros in the RHP. The numerator in $T_L(s)$ is similar to a notch filter and $T_R(s)$ is an all-pass filter. The problem becomes one of solving for U(s) in the time-domain given j(t), i.e.,

$$\mathcal{L}_2^{-1}\{U(s)\} = \mathcal{L}_2^{-1}\left\{\frac{K_{dc}^{-1}}{s} T_L(s)\, T_R(s)\, J(s)\right\} \quad . \tag{7.4}$$

The two-sided inverse Laplace Transform is not a unique mapping but is conditional on the location of the Bromwich contour. The Bromwich (Br) contour will be placed to the left of the RHP zeros and to the right of the LHP.

If we restrict the tip acceleration to be described by means of polynomials then J(s) will have the following form:

$$J(s) = \frac{1}{s^n} \sum_{m=1}^{M} P_m(s)\, e^{-s\,T_m} \quad , \tag{7.5}$$

where n is the highest order of the polynomial used to describe the tip acceleration (ex., typically cubic polynomials are used which means that n = 3) and P_m's are polynomials of order no greater than n. Further, J(s) is an entire function (i.e., no poles exist) because the jerk is restricted to finite-duration, exponential-order, and piecewise-continuous functions. However, to evaluate u(t), J(s) will be broken up into each of its m components. Each of the J's components will have up to n repeated poles at the origin.

The Br contour will be extended into two different directions depending on whether we are evaluating u(t) in the positive or negative direction of time. As shown in Fig. 7.3, two Br contours are possible: C1 and C2. Multiple poles at the origin might exist but are not shown in Fig. 7.3 (only a simple pole is shown).

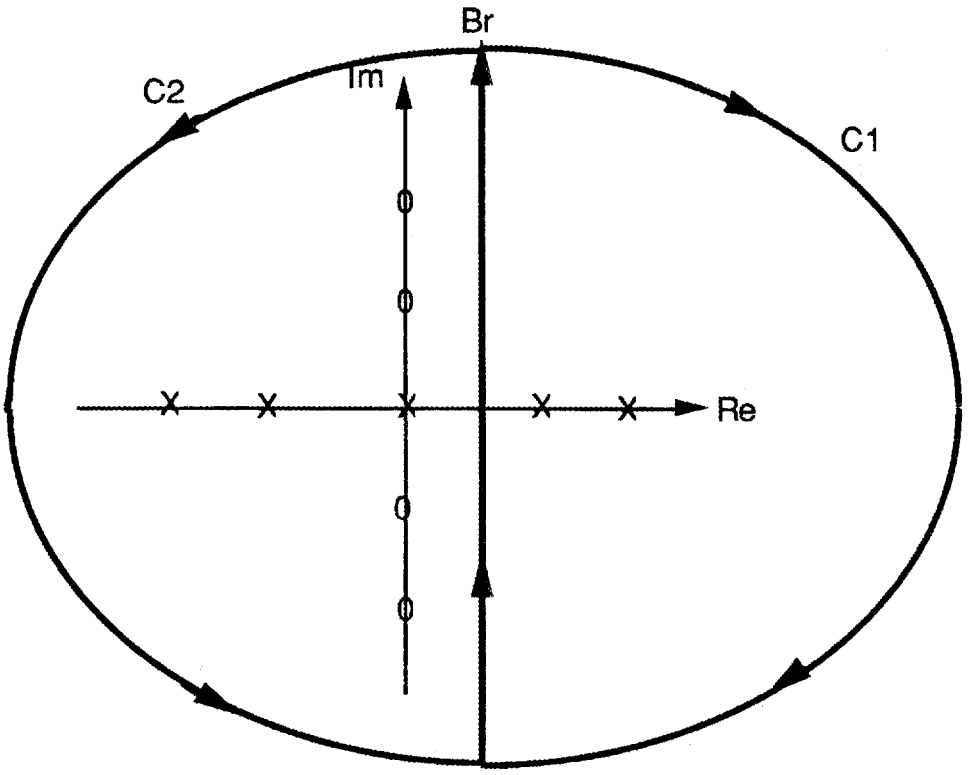

Fig. 7.3. Location of the Br contour for the d = 2 case.

The solution to Eq. (7.4) is

$$u(t) = \begin{cases} \dfrac{1}{2\pi j}\displaystyle\oint_{C_1} \dfrac{K_{dc}^{-1}}{s^{n+1}} T_L(s)\, T_R(s) \left[\sum_{m=1}^{M} P_m(s)\, e^{-s T_m} \right] e^{s t}\, ds \\[2ex] \dfrac{1}{2\pi j}\displaystyle\oint_{C_2} \dfrac{K_{dc}^{-1}}{s^{n+1}} T_L(s)\, T_R(s) \left[\sum_{m=1}^{M} P_m(s)\, e^{-s T_m} \right] e^{s t}\, ds \end{cases} \tag{7.5a}$$

or

$$u(t) = \begin{cases} \text{- sum of residues enclosed by C1} \\ \quad \text{of } \dfrac{K_{dc}^{-1}}{s} T_L(s)\, T_R(s)\, J(s) \\ \quad \text{for negative dirction of time} \\[2ex] \text{sum of residues enclosed by C2} \\ \quad \text{of } \dfrac{K_{dc}^{-1}}{s} T_L(s)\, T_R(s)\, J(s) \\ \quad \text{for positive direction of time.} \end{cases} \tag{7.5b}$$

After some manipulation, u(t) can be expressed as

$$u(t) = \begin{cases} \displaystyle\sum_{h=1}^{d} \frac{K_{dc}^{-1}}{2\, z_h^3} \frac{N_L(z_h)\left[\displaystyle\sum_{m=1}^{M} P_m(z_h)\, e^{z_h(t - T_m)}\, u_s(T_m - t)\right]}{\displaystyle\prod_{\substack{i=1 \\ i \neq h}}^{d} \left[-\left(\frac{z_h}{z_i}\right)^2 + 1\right]} \\[2ex] \displaystyle\sum_{h=1}^{d} \frac{K_{dc}^{-1}}{2\, z_h^3} \frac{N_L(-z_h)\left[\displaystyle\sum_{m=1}^{M} P_m(-z_h)\, e^{-z_h(t - T_m)}\, u_s(t - T_m)\right]}{\displaystyle\prod_{\substack{i=1 \\ i \neq h}}^{d} \left[-\left(\frac{z_h}{z_i}\right)^2 + 1\right]} \\[2ex] \qquad + \displaystyle\sum_{m=1}^{M} K_m\, u_s(t - T_m)\,, \end{cases}$$

where $u_s(t)$ is the unit step function and the K_m's are constants that do not have to be calculated from the transform. Instead, if j(t) is a continuous function then u(t) will be continuous, and any discontinuities can be corrected by looking in the negative direction of time. Otherwise, K_m must be calculated.

8. FLEXIBLE MANIPULATOR CONTROL

8.1 SUMMARY OF BASIC CONTROL APPROACHES

Trajectory following using sensory feedback has been addressed from different angles. In the literature review section, it was noted that the following basic schemes have been applied:

1. nonadaptive control,
2. adaptive and robust control,
3. high performance end-effector for dynamic compensation,
4. repetitive control system, and
5. multiple control strategies (bracing and contact control).

Only the first category will be briefly addressed in this report. A classical feedback controller will be designed using both hub and tip information. Classical methods have been selected due to their historical acceptability in industry. In addition, this will provide a baseline to which the performance of other types of controllers can be compared.

8.2 SENSOR TYPE AND LOCATION DISCUSSION

Hub position and velocity sensors are easy to implement by means of a resolver and tachometer. Tip measurements are more challenging. Tip position can be measured by means of video cameras, laser range finders, or a gyroscope. Tip velocity can be obtained by differentiating the tip positional information or directly by means of either a rate gyroscope or integrating the signal from an acceleration sensor. While obtaining accurate tip position and velocity measurements are nontrivial, for the purpose of this study they will be assumed available.

8.3 CLASSICAL CONTROLLER DESIGN

8.3.1 Plant and Controller Model

Typically, joint velocity, tip position, and tip velocity are fed back to a classical controller. Simple PD type controllers are designed such that adequate gain and phase margins are ensured against model uncertainties, sensor disturbances, unmodeled dynamics, and drive train nonlinearities. Figure 8.1 shows the block diagram model of the flexible link and controller. The inner loop is the joint or hub controller. The hub controller basically

provides joint and tip damping. The sH_u^θ joint transfer function satisfies the positive real property (because of the alternating pole-zero arrangement in the s-plane), which means that it describes a passive system. Joint velocity feedback will ensure that the inner control loop remains stable for $K_v^\theta > 0$. Without an inner-velocity feedback loop, the outer feedback loop would go unstable as can be seen from a root-locus study of this system (see **[Centinekunt,91]** for details). The control gains selected are normalized control gains based on the discussion presented in the modeling section and therefore must be adjusted for a specific uniform beam.

The N_u^y and N_u^θ transfer functions in the outer loop of Fig. 8.1 are the numerators of H_u^y and H_u^θ, respectively.

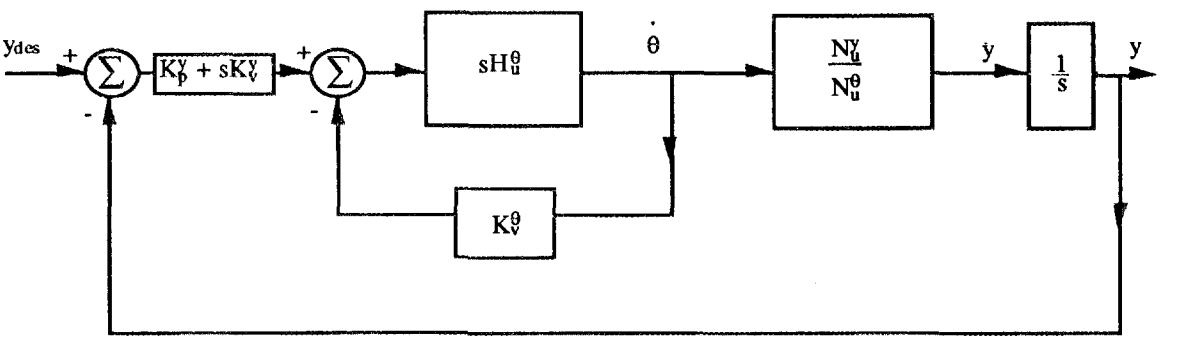

Fig. 8.1. Block diagram of flexible beam and classical controller.

8.3.2 Inner Loop Design

The inner-loop transfer function $G_{in}(s)$ is simply

$$G_{in}(s) = \frac{sH_u^\theta}{1 + s\,K_v^\theta H_u^\theta}\,, \tag{8.1}$$

and its reciprocal is

$$G_{in}^{-1}(s) = \left(sH_u^\theta\right)^{-1} + K_v^\theta\,. \tag{8.2}$$

Damping ratios of 0.01 were inserted into the transfer function because (1) lossless systems do not exist and (2) convenience of avoiding division by zero problems around resonance. A one percent damping ratio is probably far too low but was used for worse-case analysis. The inverse polar plot of $G_{in}(s)$ is shown in Fig. 8.2 for $K_v^\theta = 12$. The peak magnitude is about 1.1, which

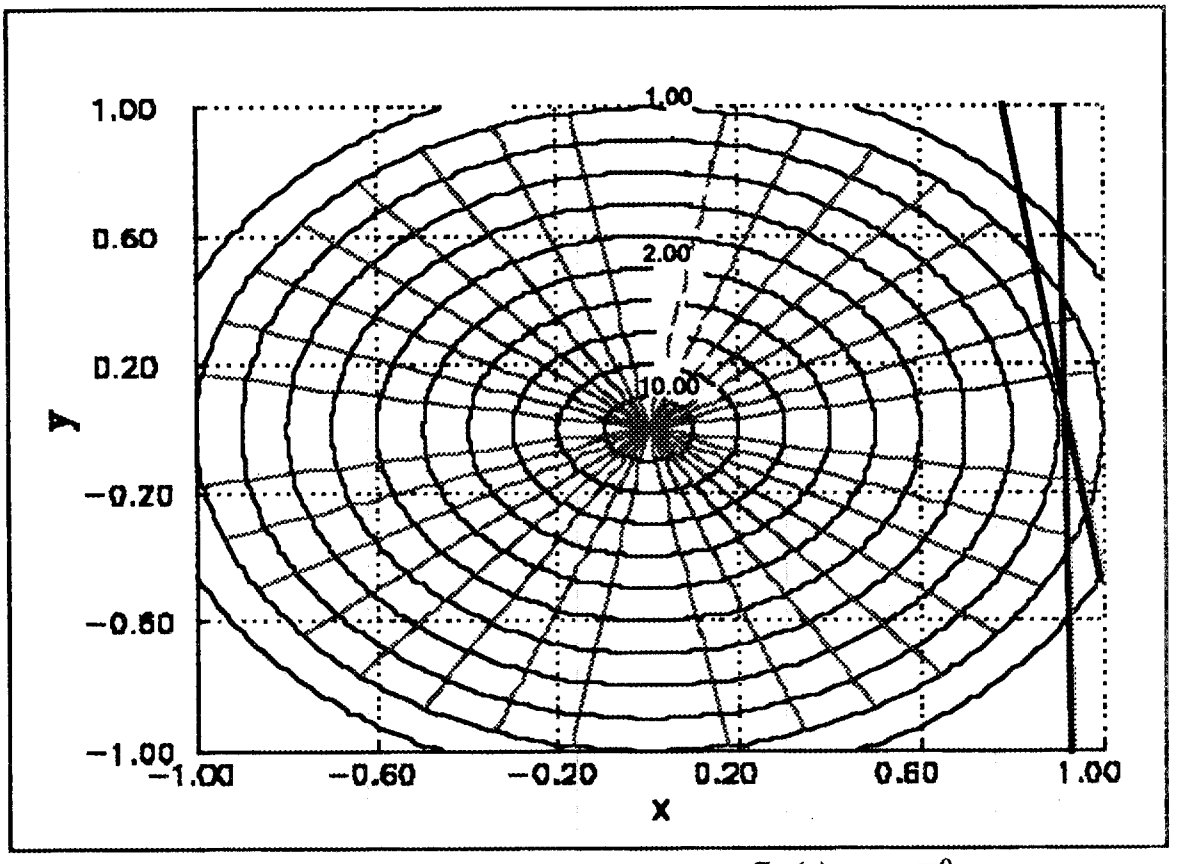

Fig. 8.2. Inner-loop inverse polar plot of $G_{in}(s)$ with $K_v^\theta = 12$.

indicates little overshoot. The bandwidth of the system is around 3.5 rad/s, which is the first nonzero zero of H_u^θ. Larger values of K_v^θ have the effect of decreasing the peak magnitude of $G_{in}(s)$ at the expense of lower bandwidth.

If an acceleration feedback term is present in conjunction with the velocity signal, higher bandwidth and lower peak magnitudes of $G_{in}(s)$ would be possible. However, acceleration feedback terms are typically noisy and present design problems which are not addressed in this study but present an interesting area of future research.

8.3.3 Outer Loop Design

The outer loop transfer function $G_{out}(s)$ is

$$G_{out}(s) = \frac{(K_p^y + s\,K_v^y)\dfrac{G_{in}}{s}\dfrac{N_u^y}{N_u^\theta}}{1 + (K_p^y + s\,K_v^y)\dfrac{G_{in}}{s}\dfrac{N_u^y}{N_u^\theta}} \quad . \tag{8.3}$$

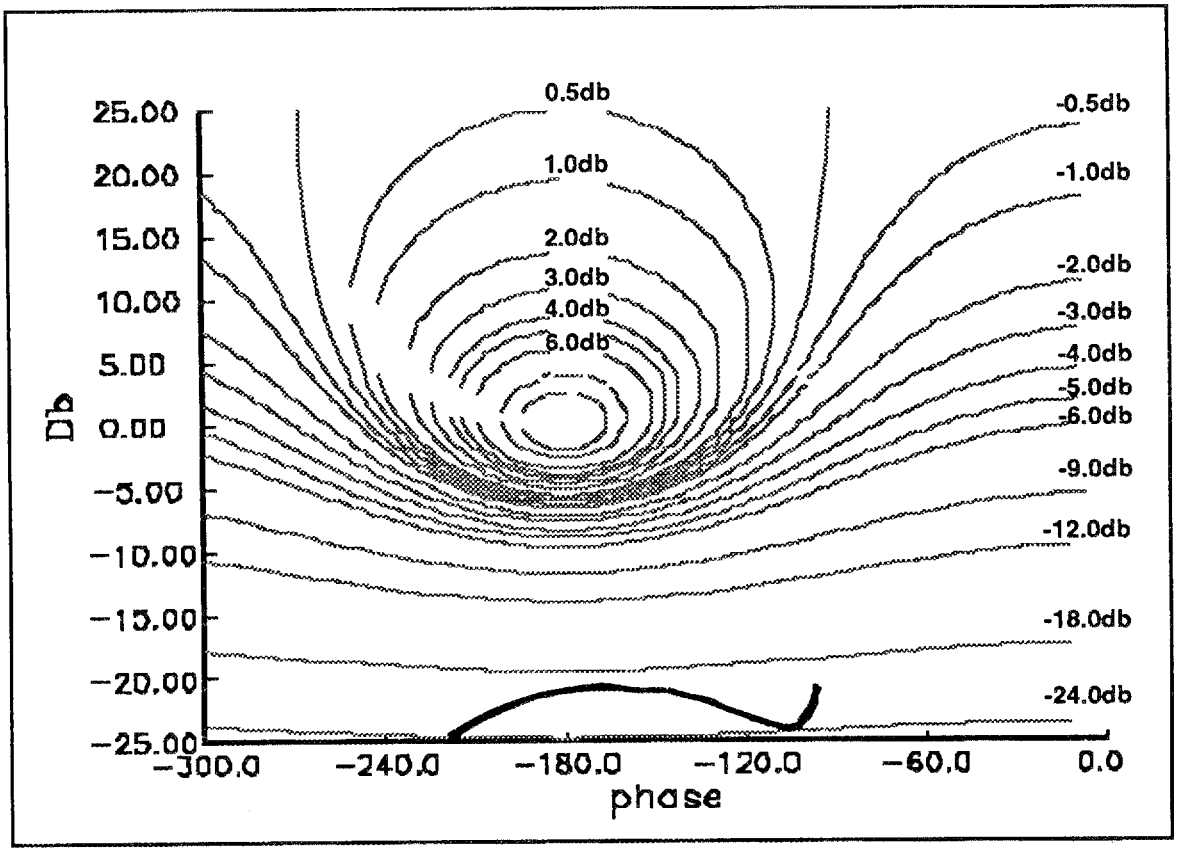

Fig. 8.3. Nichols plot of open-loop transfer function.

The open-loop transfer function is

$$\frac{G_{in}N_u^y}{sN_u^\theta}, \tag{8.4}$$

and is plotted on a Nichols chart on Fig. 8.3 where the largest magnitude of the closed loop transfer function (M_m) occurs at M_m = -19.99 dB at ω_m = 3.34 rad./s.

By iteratively adjusting the outer positional and velocity gains, the open-loop transfer function is moved as shown in Fig. 8.4, where K_p^y = 5.5 and K_v^y = 1.0. These gains will give a M_m = 0.1 dB at ω_m = 3.62 rad/s. If K_p^y is increased from 5.5 to 6, M_m will increase to 1.31 dB at ω_m = 3.61 rad/s. It is

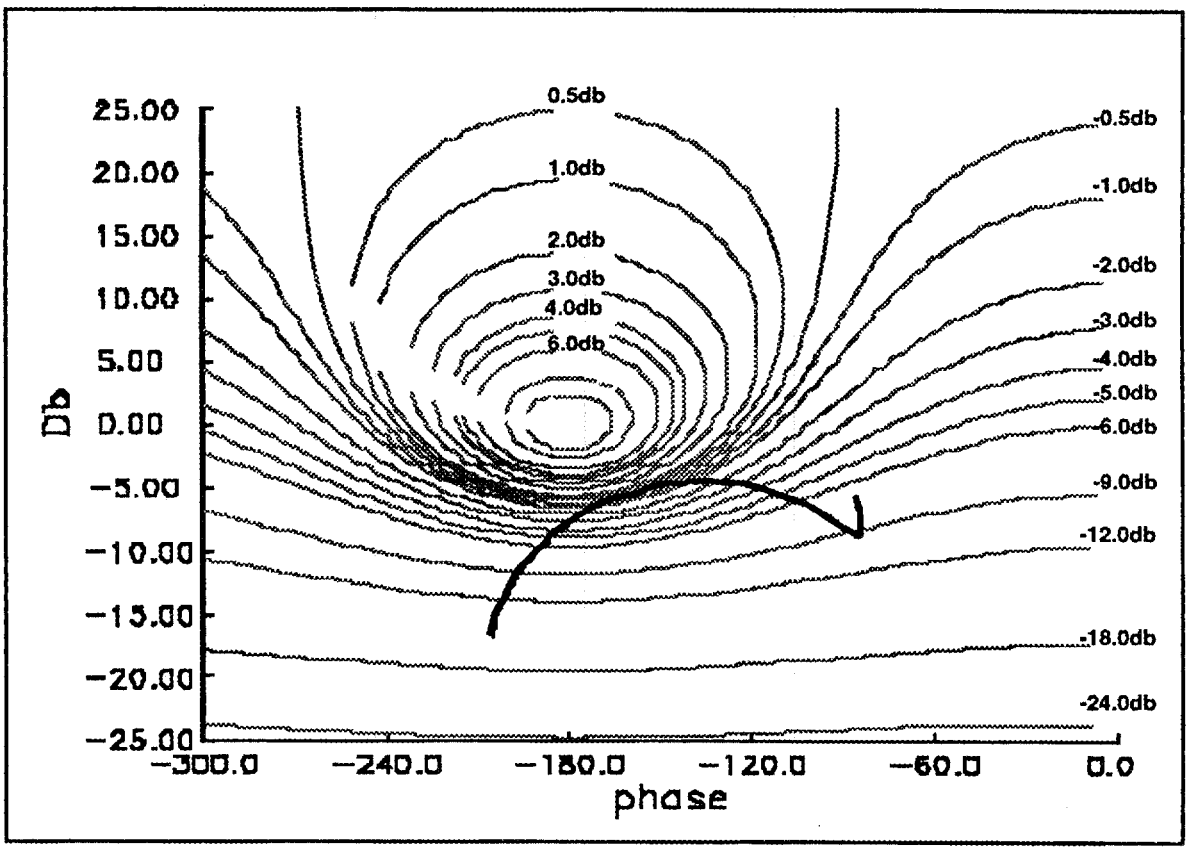

Fig. 8.4. Nichols plot for Kp = 5.5 and Kv = 1.

interesting to note that the first natural frequency for the clamped-free uniform beam is 3.516 rad/s **[Blevins, p. 108]** which according to Book is the upper bandwidth of the controller **[Centinekunt,91]**.

From Fig. 8.4, the phase and gain margins are very small. Lower values of K_p^y and K_v^y are needed to maintain appropriate levels of robustness. For $K_p^y = 4$ and $K_v^y = 1.0$, M_m = -3.4dB at ω_m = 3.6 rad/s and the phase and gain margins are within acceptable ranges as shown in Fig. 8.5.

A time simulation of a tip and hub controller is shown in Fig. 8.6 for a ramped desired tip position of 0.01 rad/s (remember that the beam has been normalized).

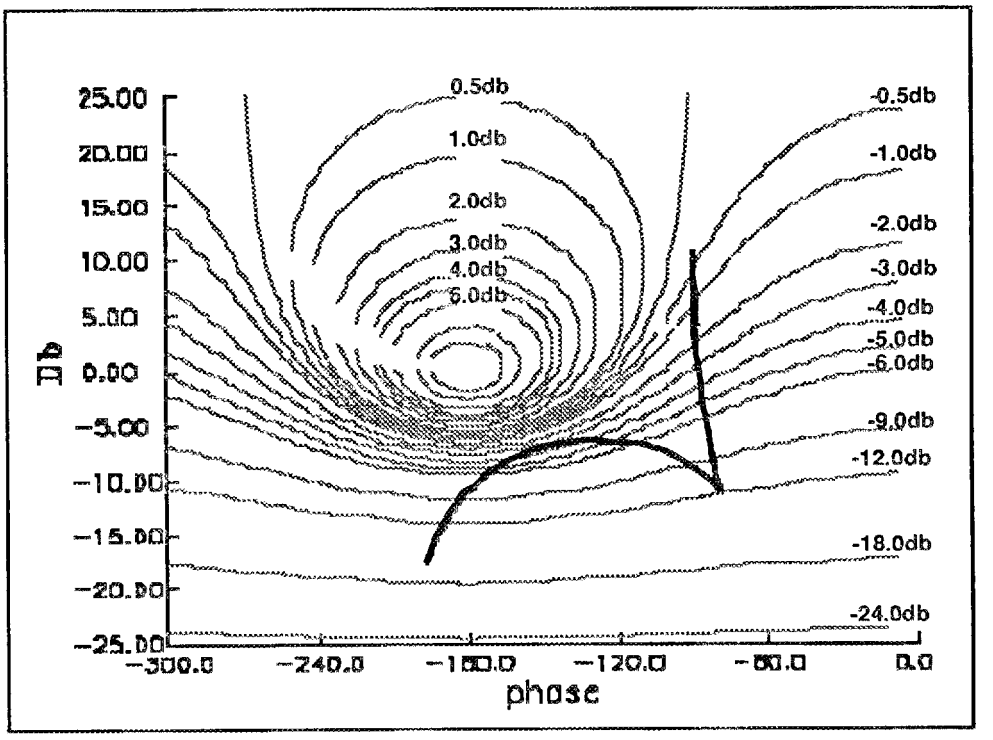

Fig. 8.5. Nichols plot for Kp = 4 and Kv = 1.

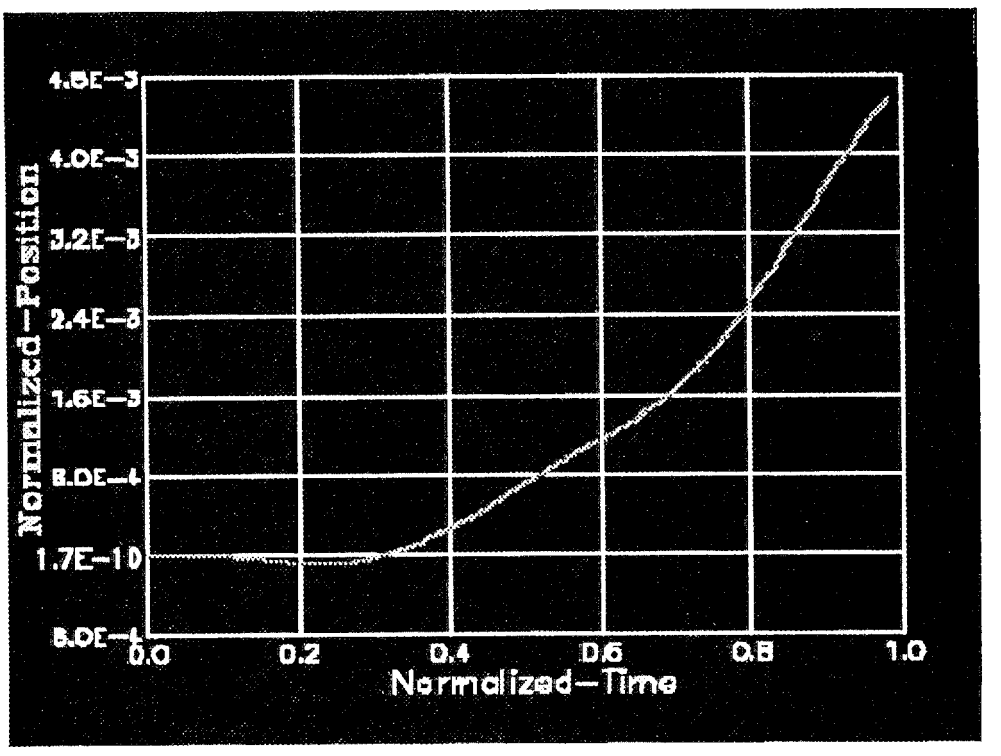

Fig. 8.6. Tip position for a ramped response.

A time simulation of a tip and hub controller is shown in Fig. 8.6 for a ramped desired tip position of 0.01 rad/s (remember that the beam has been normalized).

8.4 SUMMARY AND CONCLUSION

Using classical controller design techniques, the bandwidth of the closed loop tip controller designed was limited by the first natural frequency of the clamped free beam case. This is consistent with work by other researchers. Even the bandwidths obtained by advanced controllers are below this number. This bandwidth limitation is due to the noncollation of the actuator and sensor. A finite amount of time is required for the beam forces/moments to travel up the beam and affect the tip displacement. Due to the steep drop in dB per decade, it appears that improvements in the bandwidth of a flexible manipulator will be difficult to obtain with linear controllers and advanced controllers.

Sensitivity to parameter variables, while not shown in this report, are significant and have been observed by other researchers **[Spector,90]**. Damping is poor and must be avoided by carefully planning a trajectory that does not excite the resonant modes of the beam and controller.

9. KINEMATIC OPTIONS FOR MULTI-DEGREE-OF-FREEDOM MANIPULATORS

Kinematic design is the important first step in the conceptual design of robot manipulators, including those to be designed for ER&WM applications. Several possible manipulator kinematic configurations for waste storage tank cleanup are considered in this section .

Various actuation approaches are briefly considered, due to effects on kinematic design. Also, in order to analyze the workspace of the manipulator, constraint conditions for the range of motion of joints have to be determined. Therefore, the kinematic design of drive mechanisms are studied to obtain the optimized kinematic parameter values of drive linkages.

Given realistic joint-motion constraints, the workspaces of manipulators with different types of joints are individually optimized and then compared. An initial study of the workspaces covered by the lower degrees of freedom, not considering the wrist or tasks to be accomplished, has been performed although it is insufficient to draw a final conclusion and select the kinematic configuration. Other criteria for the selection of a manipulator kinematic configuration are briefly considered; further work in this area is needed.

9.1 JOINT ACTUATION

Hydraulic cylinders, hydraulic motors, electric motors, and electric linear actuators (ball screw drives) can be considered for actuation of the joints for a long-reach manipulator for ER&WM applications. In this preliminary investigation addressing only the primary joints, the use of electric motors is not considered because of the large required torques. A torque capacity in the order of 80,000 ft-lb will be required at the first pitch joint. If hydraulic motors are used for revolute joints, there will be no limit of the range of the motion, but the joint motion angular rate will be slower and the weight will be heavier because of reduction gears than if hydraulic cylinders are used. Therefore, hydraulic cylinders will be the most likely actuators to be chosen for revolute and prismatic joints.

9.2 DRIVE LINKAGE STUDIES

If a hydraulic cylinder is used as an actuator of a revolute joint and no additional mechanisms or drives are included, a reasonable joint motion constraint has to be defined for the workspace analysis The design issue is to find the optimum joint linkage configuration having a maximum joint angle

range for a given minimum actuation torque throughout the joint range. In order to minimize the actuator weight, a relatively constant actuation torque throughout the joint range is desirable. First, the relation between the hydraulic cylinder length L1 and the attachment point locations defined as L2 and L3 of the linkage configuration in Fig 9.1, which allows the maximum range of the joint motion, is investigated. Second, a near-optimum linkage configuration is selected by a compromise between the maximum joint angle range and the actuation torque distribution, since the joint linkage configuration for maximum joint-angle range gives worst actuating torque distribution for the joint range, and the joint linkage configuration for the maximum torque distribution gives the minimum joint angle range.

9.2.1 Analysis

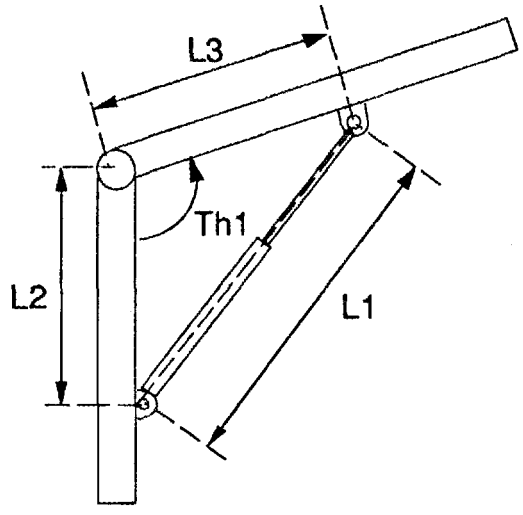

Fig. 9.1. Joint linkage configuration for a hydraulic cylinder.

In the following analysis, it is assumed that the hydraulic cylinder can be extended up to 80% of the original length. Commercial, single-extension, hydraulic cylinders extend 70 to 90% of their original length, depending on the cylinder length. Therefore, the hydraulic actuator length L1 must satisfy

$$L1min \leq L1 \leq L1max ,$$

where L1min ≡ L, L1max = alpha *L, and alpha is assumed to be 1.8.

The maximum joint angle range can be calculated by calculating the minimum joint angle, Th1min and the maximum joint angle, Th1max for various values of L2 and L3:

$$Th1min = \cos^{-1}((L2^2 + L3^2 - L1min^2)/2*L2*L3),$$

$$Th1max = \cos^{-1}((L2^2 + L3^2 - L1max^2)/2*L2*L3).$$

Table 9.1 lists the joint angle range for various values of L2 and L3, assuming L1min is 1 and L1max is 1.8.

Table 9.1. Joint angle range vs L2 and L3

Joint angle range (degrees)	L2 (L = 1)	L3 (L = 1)
154.91	0.41	1.4
159.62		1.41
147.41	0.42	1.39
144.88		1.4
144.72		1.41
151.39		1.42
142.45	0.43	1.38
139.09		1.39
137.42		1.4
136.95		1.41
137.91		1.42
145.23		1.43
138.56	0.44	1.37
134.82		1.38
132.61		1.39
131.31		1.4
130.78		1.41
131.05		1.42
132.53		1.43
140.15		1.44
135.32	0.45	1.36
131.36		1.37
135.76		1.45
132.52	0.46	1.35
131.89		1.46
130.05	0.47	1.42

The limit value occurs at L2 = 0.4 and L3 = 1.4 for L = 1 for the maximum joint angle range. In general, the limit values of L2 and L3 in terms of the maximum and minimum values of L1 are:

$$L2 = (L1max+L1min)/2,$$

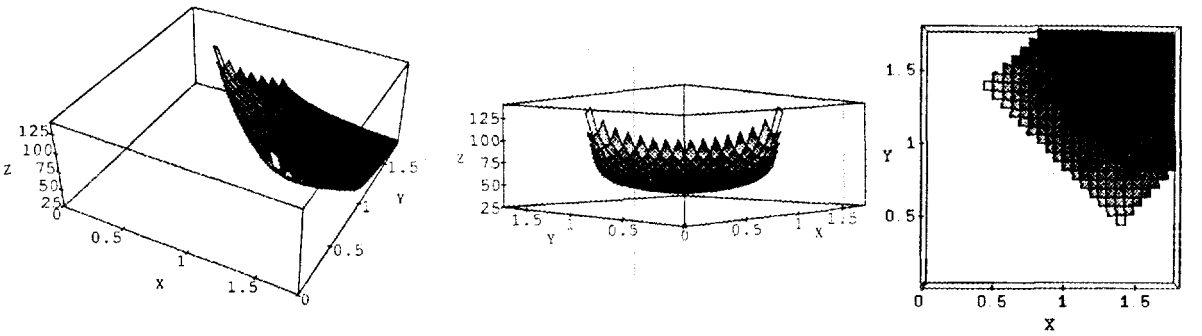

Fig. 9.2. Maximum range of the joint angle motion
X axis : L2, Y axis : L3, Z axis: joint angle range (degrees).

The joint torque capacity is directly related to the joint torque arm length, Hc, which is given by:

$$Hc = 2/\{L1*Sqrt[S\ (S-L1)\ (S-L2)\ (S-L3)]\},$$

where

$$S = (L1+L2+L3)/2\ .$$

The torque arm length is calculated effectively as a function of the joint angle by changing the lengths L1 and L2. L3 changes dependently. As L3 approaches L1max-L2, a maximum joint angle is obtained for the value of L2. Figure 9.3 depicts the torque arm length distribution as a function of the hydraulic cylinder length, L1, and L2. Figure 9.4 depicts the joint torque for different combinations of L2 and L3.

9.2.2 Conclusion

For commercially available hydraulic cranes, a 105 to 140° joint motion range is commonly used. From the analysis, the limiting joint motion range is 180° (0 to 180°), the range practically available is between 100 and 155°, and the optimum range considering the torque distribution is 135° (30 to 165°).

For a revolute joint actuated by a hydraulic cylinder with a stroke of 80% of the minimum length (a length varying between 1 and 1.8), a configuration having L2 = 0.45 and L3 = 1.36 yields a 135° joint angle range and a very suitable actuating torque distribution. Therefore, in the workspace analysis and comparisons, a 135° joint range is used for the joint angle constraint condition.

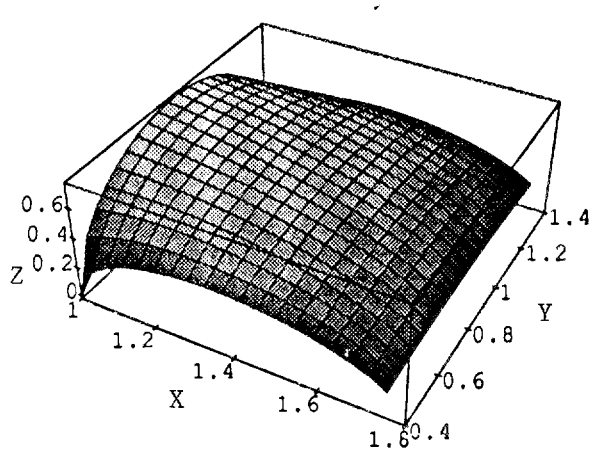

Fig. 9.3. Joint torque distribution.
X axis: L1 (hydraulic cylinder length),
Y axis: L2,
Z axis: Torque arm length.

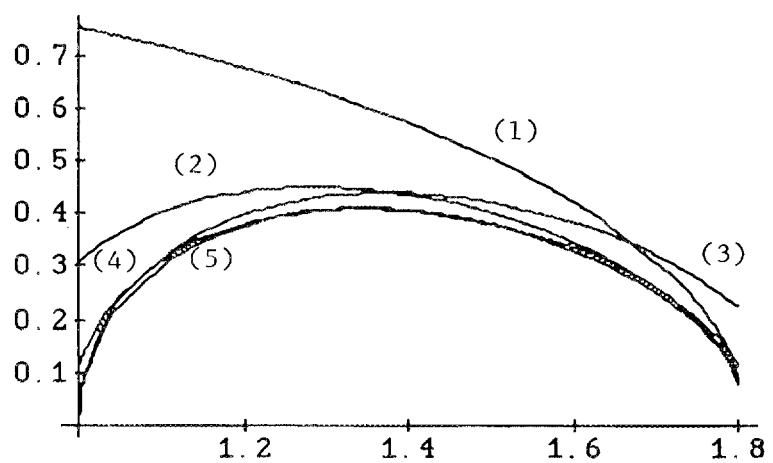

Fig. 9.4. Joint torque for different linkage configurations.
X axis: L1 (hydraulic cylinder actuator),
Y axis: torque arm length.

1. L2 = 0.9, L3 = 0.91
2. L2 = 0.45, L3 = 1.36 (best case)
3. L2 = 0.41, L3 = 1.4
4. L2 = 0.41, L3 = 1.41
5. L2 = 0.44, L3 = 1.44

Limiting values of L2 and L3 depend on the assumed hydraulic cylinder extension ratio, alpha. These occur at L2 = (L1max+L1min)/2, L3 = (L1max-L1min)/2. This gives some guidance for the joint design of the hydraulic cylinder actuator link.

9.3 SIMPLE STRUCTURES APPROACHES - A COMPARISON OF WORKSPACES

In this section, three robot configurations are studied to determine the optimum individual link lengths and the minimum overall arm length required to cover the workspace. The robots considered all have a base extension (prismatic joint) which allows lowering the arm into the waste storage tank to various elevations. The three configurations vary in the remaining positioning joints. (Wrist configurations are not considered in this initial study.) These include a roll-pitch-pitch (RPP) manipulator, a roll-pitch-extend (RPE) manipulator, and a roll-pitch-pitch-extend (RPPE) manipulator. Since the first joint (after the common base extension) is revolute, the search for the 3D workspace can be reduced to the study of the area in a plane normal to the axis of the roll joint.

Note that the term tank height refers to the height of the lined portion of the tank or the cylindrical portion of the tank. The tanks have additional height in the domed top. For simplicity, it is assumed that the tanks have heights equal to their radii. The same methodology applies to tanks with other aspect ratios.

9.3.1 Optimization of the Workspace of a Revolute Joint Robot.

The volume of the workspace of a general robot is to be optimized in this section. All of the robots being studied have an initial extension and a revolute joint. Because of the revolute joint, the workspace is a volume of revolution. As it is shown in the Fig. 9.5, the workspace of a robot with an initial rotary (roll) joint is produced by rotating an area about the roll joint axis. The area to be rotated is in a plane that contains the axis of rotation. Thus, covering the area means covering all of the workspace. In the discussions that follow, the workspace area of revolution is considered to be $0 \le r \le 1$ and $-1 \le y \le 0$, not counting reaching the top surface of the tank.

Note that the storage tanks have the same radial symmetry as the workspace produced by a robot with a first rotary joint. This is a principal consideration when designing the long-reach manipulator.

9.3.2. RPP Manipulator Workspace Optimization

For an RPP manipulator, the area that creates the workspace is found for a fixed value of the first rotary joint. This area is given by

$$A = L_1 L_2 (\theta_{1max} - \theta_{1min}) (\cos(\theta_{2max}) - \cos(\theta_{2min})),$$

where L1 and θ_1 are the length and angle of the first Pitch joint, and L2 and θ_2 are those of the second link.

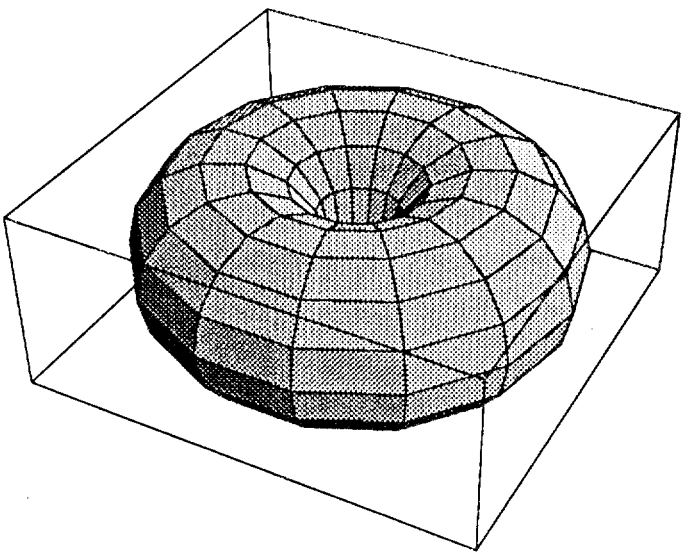

Fig. 9.5. Symmetric workspace of a robot with an initial rotational joint.

Thus the variables that can be used in the optimization of the area reached by an RPP manipulator are: (1) the two link lengths (L_1 and L_2), (2) the constraint range of the first pitch joint($q1max$ - $q1min$), and (3) the angular constraints of the second pitch joint($q2max$ and $q2min$).

9.3.2.1 Workspace as a Function of Angular Constraints and Lengths

The relation between the area covered by the two-link RPP robot, the ratio between the two link lengths, and the range of the angular constraint for each joint can be plotted using the following coordinates: (1) Z-direction for

area, (2) Y-direction for the ratio alpha = L1/(L1 + L2), and (3) X-direction for the angular constraint range (in degrees).

In order to make it easier to compare results, the following conditions were used:

1. the length of the manipulator, L1 + L2, is normalized to one. (Thus, whatever values found for the lengths will be later multiplied by the diameter of the storage tank to find the real values.),
2. the angular constraints of both angles are equal, and
3. $\theta_{2max} = 0$.

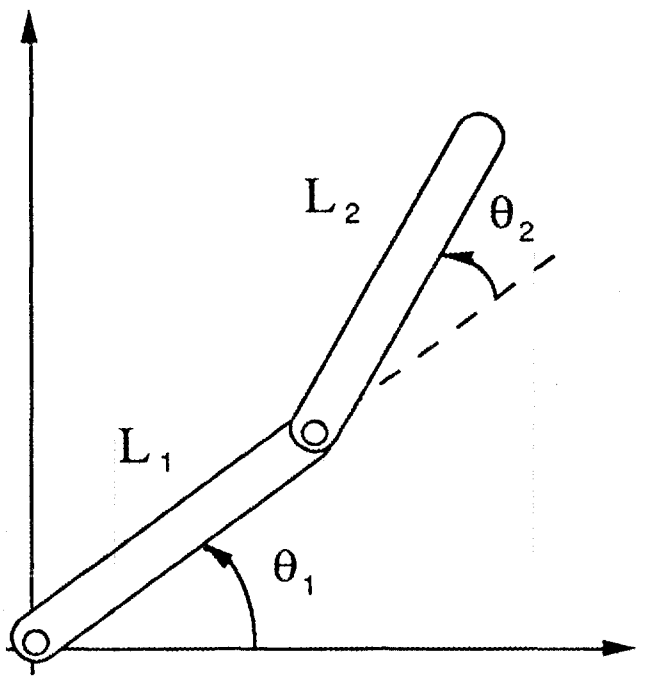

Fig. 9.6. Two-link, planar, revolute joint robot to which an RPP robot can be reduced to study its workspace.

The area can be plotted as a function of the ratio alpha and the angular constraints as shown in Fig. 9.7 from two different points of view.

As it can be seen, the maximum area is obtained approximately for alpha = 0.5. This means that L1, the length of the first link, should be equal to L2, the length of the second one. This can be proven to be true

mathematically using the Lagrangian optimization technique. For an objective function:

$$A(L1, L2) = L1 \ L2 \ K,$$

subject to

$$L1 + L2 - L = 0,$$

where

$$K = (\theta 1max - \theta 1min) \ (Cos(\theta 2max) - Cos(\theta 2min)),$$

the Lagrange function is:

$$L(L1, L2, \lambda_0, \lambda_1) = \lambda_0 \, L1 \, L2 \, K + \lambda_1 \, (L1 + L2 - L) \, .$$

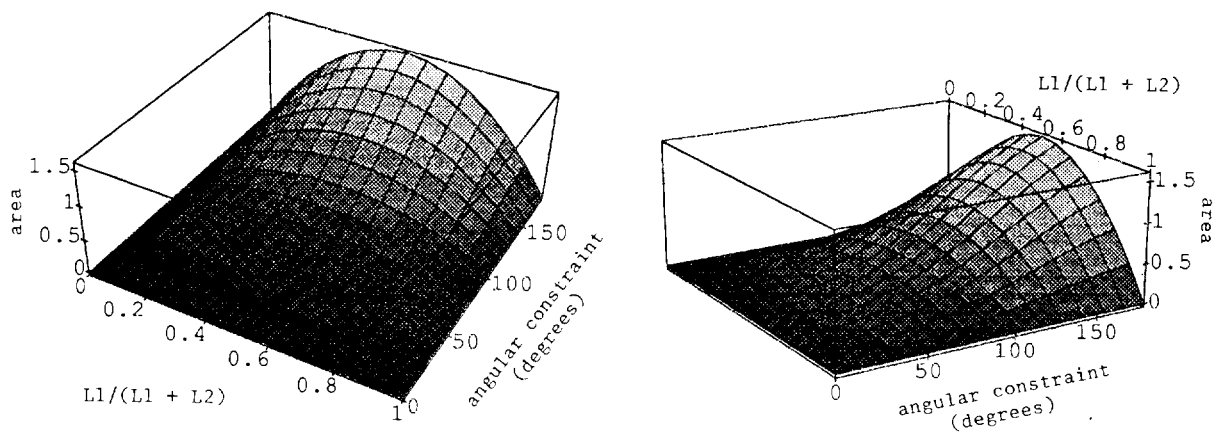

Fig. 9.7. Two different points of view of the area of the workspace of an RPP robot as a function of the relation between its lengths and its angular constraints.

The case $\lambda_0 = 0$ does not yield a valid solution, but the case $\lambda_0 = 1$ yields a maximum for the objective function when L1 is equal to L2. Furthermore, for any range of the constraint, the maximum area is found for Alpha = 1/2. That means that the maximum reached area is for L1 = L2.

Table 9.2 indicates how the area increases just as function of the range of the angular constraint having L1 = L2.

Table 9.2. Percent change in workspace area

Area	angular constr.(degrees)	% change
0.0	0.	0.000
0.004	10.	1.000
0.030	36.	0.872
0.097	54.	0.691
0.217	72.	0.553
0.393	90.	0.447
0.617	108.	0.363
0.873	126.	0.293
1.137	144.	0.232
1.379	162.	0.176
1.571	180.	0.122

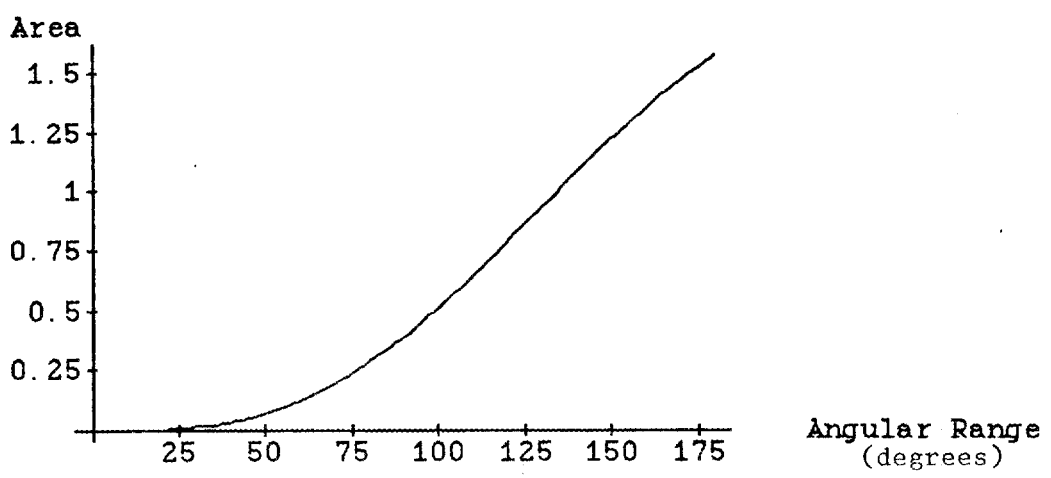

Fig. 9.8. Area of an RPP manipulator with $L_1 = L_2$ as a function of the angular range constraints.

From 0 to 75°, the area increases very quickly with the increase of the angular constraint range. Between 75 and 140° the curve is almost linear. And then, the inflexion point between 140 and 150° indicates that after this point, improving the angular range does not improve the area as much as before.

This is coincident with the data obtained from industrial robots. The typical maximum range for an industrial robot with rotational joints is about 140°.

The conclusion is that in order to optimize the workspace of an RPP robot, L_1 should be equal to L_2 and the angular constraints $(\theta_{1max} - \theta_{1min})$ and $(\theta_{2max} - \theta_{2min})$ should be equal to 140°.

9.3.2.2 Area and Volume Covered by an RPP Manipulator

One of the fundamental objectives of the robot is that its workspace must cover all of the storage tank. The robot has to be able to reach any point inside the tank, but at the same time we would like the robot to be as short as possible. Thus the working area has to be covered minimizing the wasted work area as much as possible.

In order to make it easier to compare results, the dimensions of the storage tank will be normalized. The radius and the height of the tank will be considered to be equal and given a value of 1 on the next plots. Thus the boxes on the next plots show the dimensions of the tank. The storage tank will be between 0 and -1 on the y direction, and between 0 and 1 on the x direction. A plot of the area covered by an RPP robot in the plane defined by the first joint using $L_1 = L_2$ and $(\theta_{1max} - \theta_{1min}) = (\theta_{2max} - \theta_{2min}) = 140°$ is shown in Fig. 9.9.

Figure 9.10 shows the same plot when $L_1 = L_2$, $(\theta_{1max} - \theta_{1min}) = 140°$, and $(\theta_{2max} - \theta_{2min}) = 280°$.

The robot is supported by a column that can be considered as a discrete degree of freedom. This column acts as a prismatic joint, with its length defining the position of the elbow of the manipulator. Because this column is not as easy to move as the rest of the joints, its use will be limited to two or three different positions. With the inclusion of the effect of this discrete degree of freedom, Fig. 9.11 shows how the tank workspace is covered by the robot. Note that the tank is confined between 0 and -1 in the y direction (the height of the lined or cylindrical portion of the tank), and between 0 and 1 in the x direction (the radius of the tank), not considering the volume in the dome covering the tank. It was found graphically that a good choice for three discrete positions of the column was 0.25, -0.25, and -0.75 % of the height of the tank. It is likely that some of the upper part of the cylindrical portion of the tank shown as reachable in Fig. 9.11 cannot in fact be reached due to interference between the elbow and the top of the tank with the manipulator in the elbow up configuration.

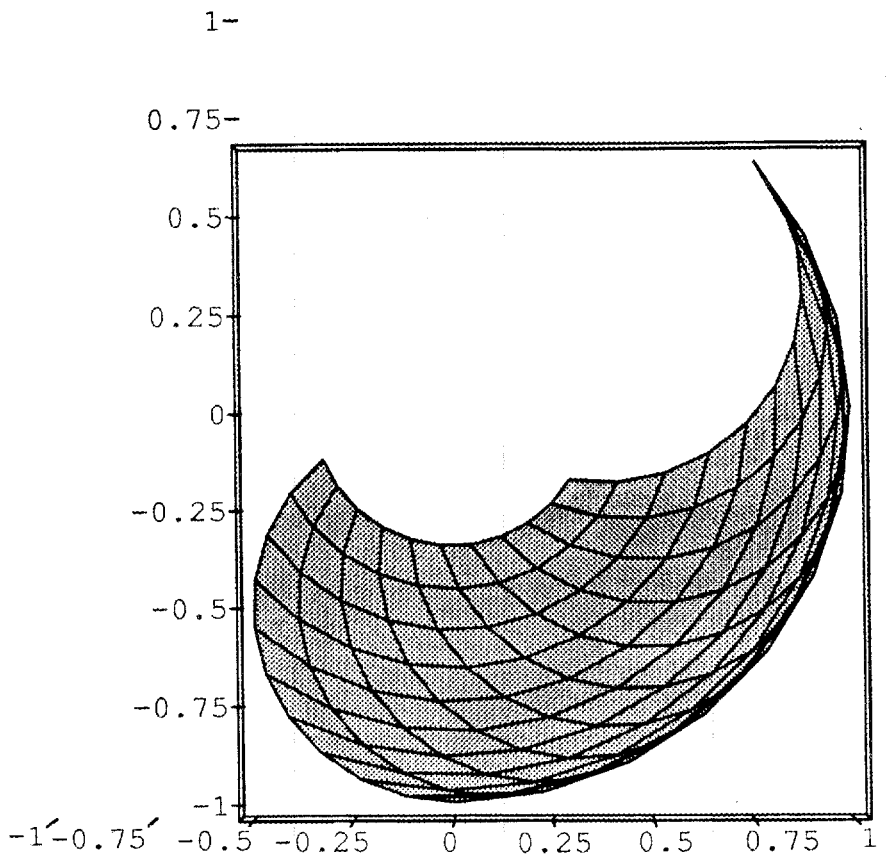

Fig. 9.9. Workspace of an RPP robot when $L_1 = L_2$ and $(\theta_{1max} - \theta_{1min}) = (\theta_{2max} - \theta_{2min}) = 140°$.

9.3.2.3 Elbow Up, Elbow Down on an RPP Manipulator

Note that the top of the tank is not fully reached with robot configuration and constraints shown in Fig. 9.11. The constraints used before assume that the elbow of the robot is always going to be up as shown in Fig. 9.12a. In order to reach all of the top of the tank, the elbow has to be allowed to be down too, as shown in Fig. 9.12b. The reason is that to reach the top with the elbow up, the elbow must be be outside of the tank, a condition that cannot be allowed.

When the elbow is allowed to be up and down, Fig. 9.13 shows the workspace as Fig. 9.11 showed for only elbow up.

Note that by allowing the elbow to be up and down, the second joint of the robot has to be able to cross the zero angle position. This is a singular position thus the manipulator cannot go through it freely. Some industrial

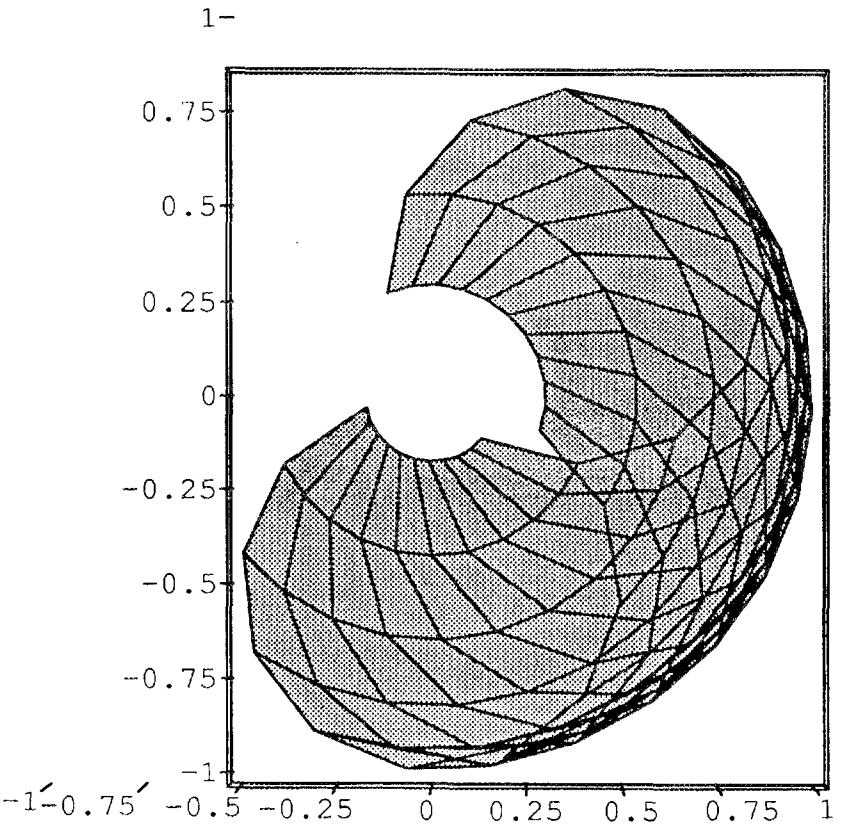

Fig. 9.10. Workspace of an RPP robot when $L_1 = L_2$, $(\theta_{1max} - \theta_{1min}) = 140°$, and $(\theta_{2max} - \theta_{2min}) = 280°$.

robots use their own inertia to go through that singular point. Such a technique cannot be used in a long manipulator. An extra actuator would have to be installed to allow the two configurations. The extra actuator could be very small, and it might be a hydraulic actuator with only two positions to place the manipulator in either the elbow up position or the elbow down position. Most of the time the manipulator would be used with the elbow up, and it would be designed to have maximum mechanical advantage in that configuration.

9.3.2.4 Conclusions for an RPP Manipulator Optimization

In order to assure that boundary singularities are not encountered, the total length of the manipulator must be greater than the diameter of the waste storage tank. A reasonable assumption would be approximately 110%

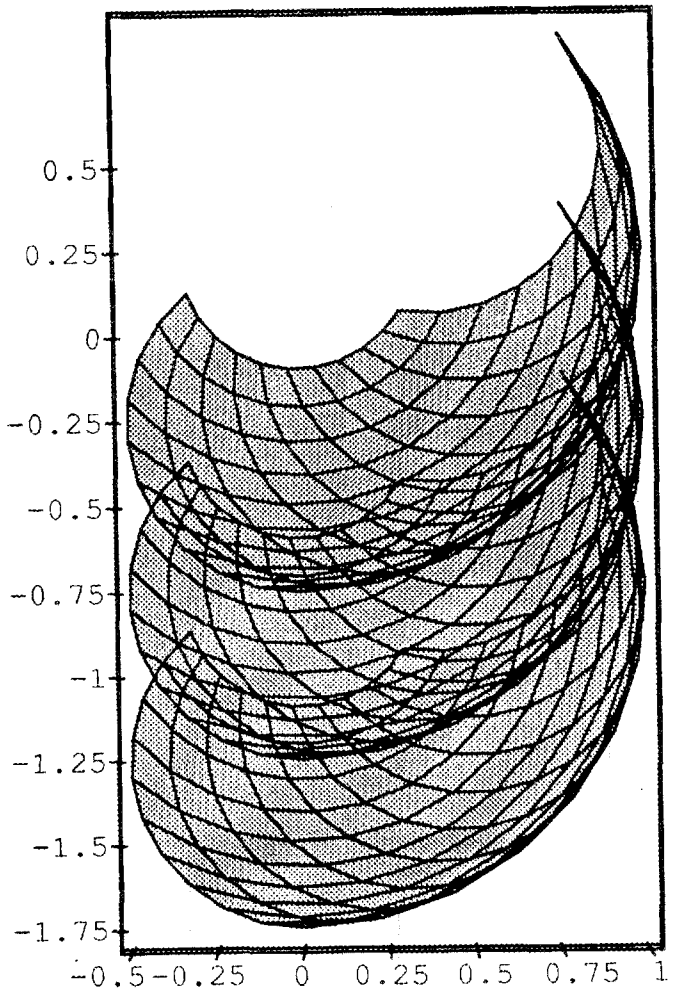

Fig. 9.11. Workspace of an RPP robot when $L_1 = L_2$ and three discrete positions for the shoulder at (0,.25), (0, -.25), and (0,-.75) and the height of the tank equal to 1.

of the diameter of the tank. Since the two links must be of equal length for a maximum volume coverage, L1 and L2 should be 55% of the diameter of the tank. The angular constraints for the first pitch degree of freedom are

$$\theta_{1min} = -90°,$$
$$\theta_{1max} = 40°.$$

For the second pitch degree of freedom, the angular constraints if the top of the tank does not need to be reached are

$$\theta_{2min} = -140°,$$
$$\theta_{2max} = 0°.$$

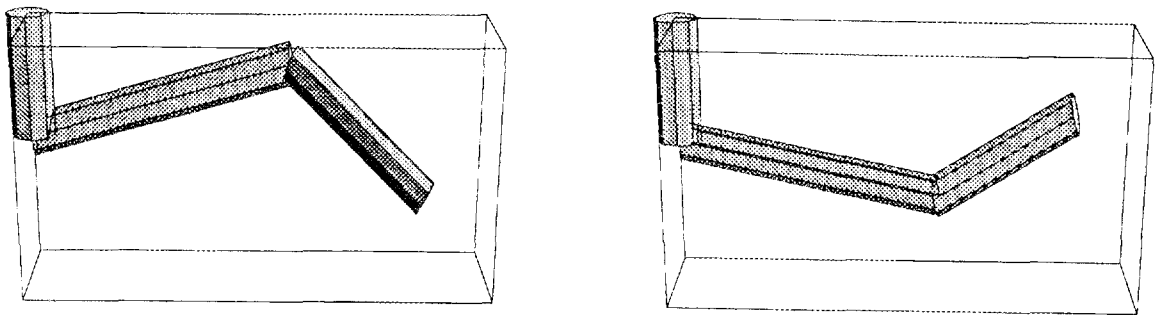

(a) Elbow up. (b) Elbow down.

Fig. 9.12. An RPP robot with the elbow up and down.

If top of the tank needs to be reached, the angular constraints for the second pitch degree of freedom are

$$\theta_{2min} = -140°,$$
$$\theta_{2max} = 140°.$$

Three discrete positions for the column at 25, -40, and -70% of the height of the tank allow full coverage of the tank with the manipulator.

9.3.3. RPE Manipulator Workspace Optimization

For an RPE manipulator, the area that creates the workspace is found for a fixed value of the first rotary joint. This area is given by

$$A = \frac{(L_{max})^2 - (L_{min})^2}{2} \quad (\theta_{max} - \theta_{min}) ,$$

where L_{max} and L_{min} are the maximum and minimum lengths of the extension link, and θ_{max} and θ_{min} are the maximum and minimum angles of the pitch degree of freedom.

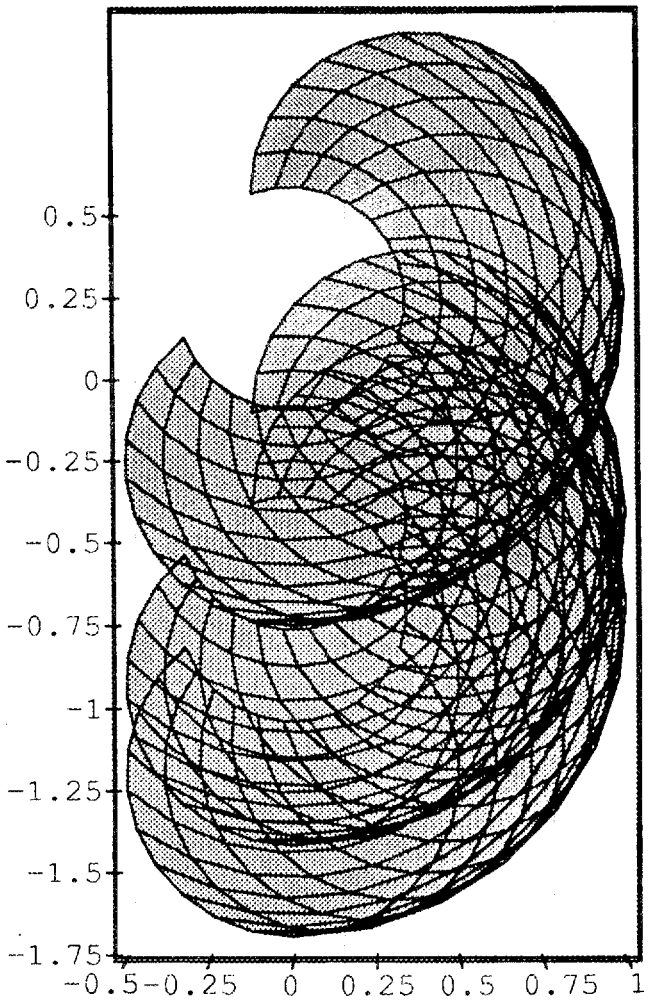

Fig. 9.13. Workspace of an RPP robot when $L_1 = L_2$, three discrete positions for the shoulder at (0,.25), (0, -.40), and (0,-.70) and the height of the tank is equal to 1. (The elbow is allowed to be up and down.)

Optimization of this area in function of the lengths of the robot is not viable. The solution for the optimization will be $L_{min} = 0$ and $L_{max} = L$.

9.3.3.1 Two and Three Stages for an RPE Manipulator.

Mechanical limitations constrain the minimum length of the RPE manipulator. Every extension stage has to be smaller than the preceding stage. Using the same technique used with the RPP manipulator, we will normalize the length of the RPE robot making $L_{max} = 1$.

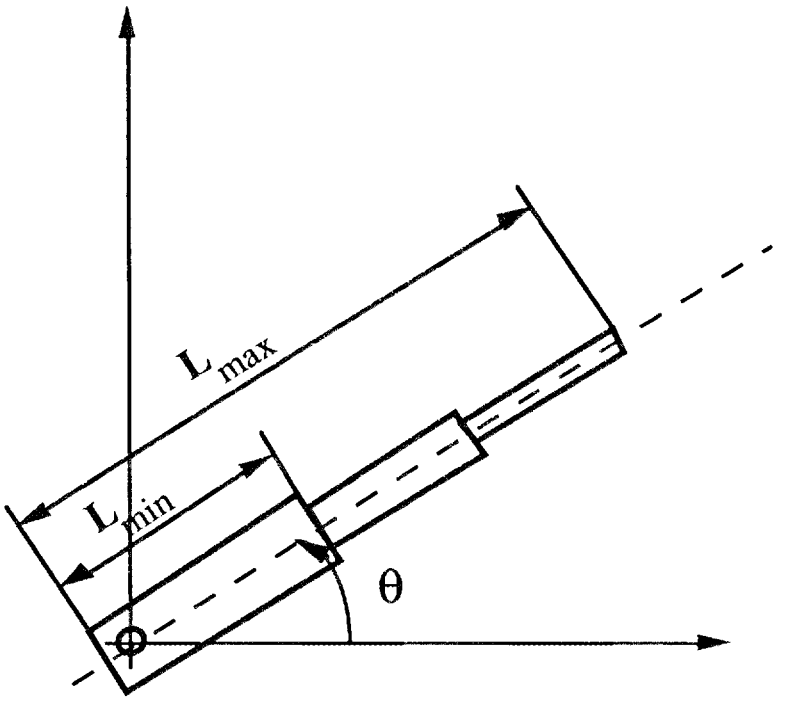

Fig. 9.14. One link planar extension robot to which an RPE robot can be reduced to study its workspace.

If two extension stages are used for this robot configuration, L_{min} can never be smaller than $L_{max}/2$. In fact, industrial robots use an extension of 80%, which makes

$$L_{max} = 1,$$
$$L_{min} = 0.55.$$

Using two stages and three discrete locations for the column of the robot, as were used with the RPP configuration on Figs. 9.11 and 9.13, it is easy to see that not all of the volume of the tank is covered by the robot in this configuration. Figure 9.15 shows the RPE robot for three discrete positions of the column at 0.25, -0.25, and -0.75 % of the height of the tank.

If three extension stages are used for this robot configuration, L_{min} can never be bigger than $L_{max}/2$. Industrial robots use two extensions of 80%, which makes

$$L_{max} = 1,$$
$$L_{med} = 0.74,$$
$$L_{min} = 0.41.$$

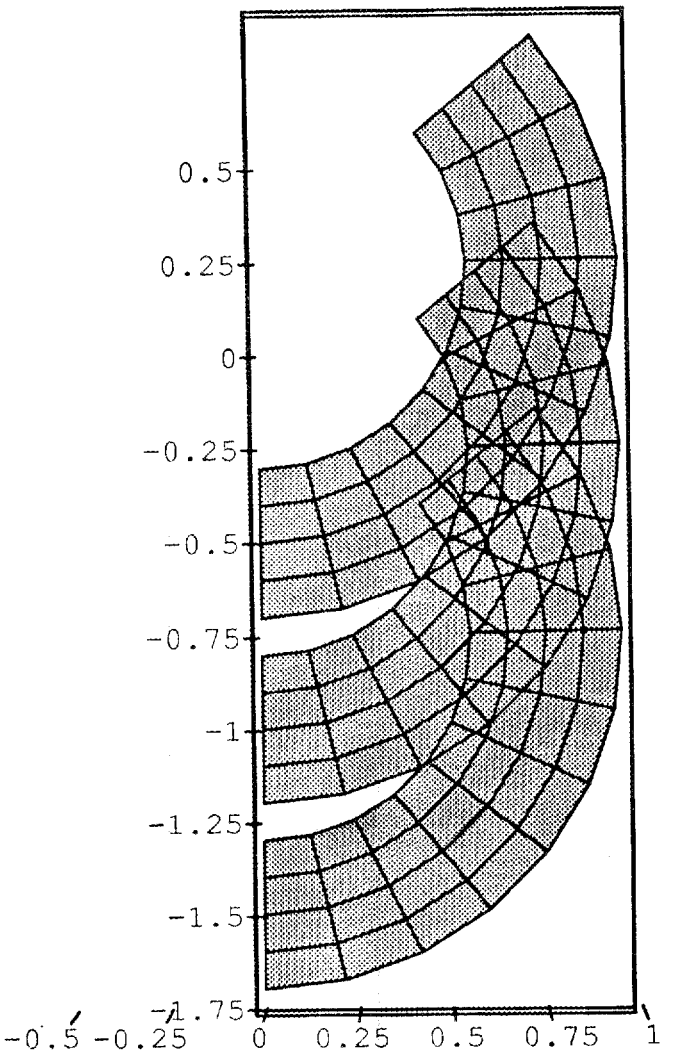

Fig. 9.15. Workspace of an RPE robot with two stages and three discrete positions for the shoulder at (0,.25), (0, -.25), and (0,-.75), given a tank height of 1.

Using three stages and three discrete locations for the column of the robot, as were used on Figs. 9.11, 9.13 and 9.15, almost all of the volume of the tank is covered. Figure 9.16 shows an RPE robot for three discrete positions of the column at 0.25, -0.25, and -0.75% of the height of the tank.

9.3.3.2 Conclusions for RPE Manipulator Optimization

As in the case of the RPP manipulator, in order to assure that boundary singularities are not encountered, the total length of the manipulator must be greater than the diameter of the waste storage tank. A reasonable assumption

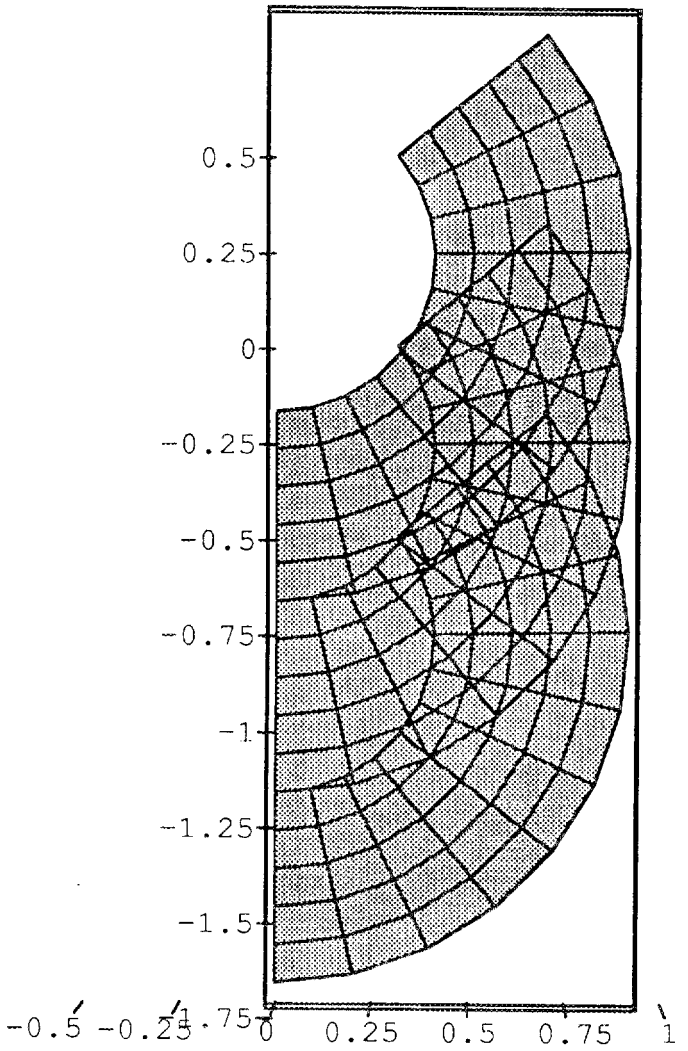

Fig. 9.16. Workspace of an RPE robot with three stages and three discrete positions for the shoulder at (0,.25), (0, -.25), and (0,-.75), given a tank eight of one.

would be approximately 110% of the diameter of the tank. With this maximum length, ~3.5% of the area of the tank is not reachable and ~50% of the top of the tank is also not reachable. The pitch degree of freedom has the following angular constraints:

$$\theta_{min} = -90°,$$
$$\theta_{max} = 40°.$$

At least three stages of 80% extension are necessary with the following overall link lengths:

$$L_{max} = 1,$$
$$L_{med} = 0.74,$$
$$L_{min} = 0.41.$$

The three discrete positions for the column chosen allow nearly full coverage of the tank with the RPE manipulator. These are at 25, -25, and -75% of the height of the tank. A small volume near the center is not covered.

9.3.4. RPPE Manipulator Workspace

A graphical comparison has been done for an RPPE manipulator. The extra degree of freedom will allow the robot to avoid singularities and to make possible some trajectories that in other cases could be very difficult or impossible to control. In particular, the last extension will allow the end effector of the robot to move in a straight line along its degree of freedom. This movement may be useful for grasping objects or for cleaning an area with a vacuum system.

9.3.4.1 Graphical Analysis of Workspace

An optimization of the workspace has been done graphically. The last extension has the same mechanical impediments that were presented in the RPE case. Furthermore, three stages of 80% increase have been used to make the extension more useful.

Finally, a good configuration able to cover more than 95% of the workspace was considered to be for:

$$L_1 = 0.3,$$
$$L_{2min} = 0.29,$$
$$L_{2med} = 0.52,$$
$$L_{2max} = 0.7.$$

The total length of the manipulator will still be in this case equal to one ($L_1 + L_{2max} = 1$). In this way, the graphical results will be comparable with those of the robot configurations presented before.

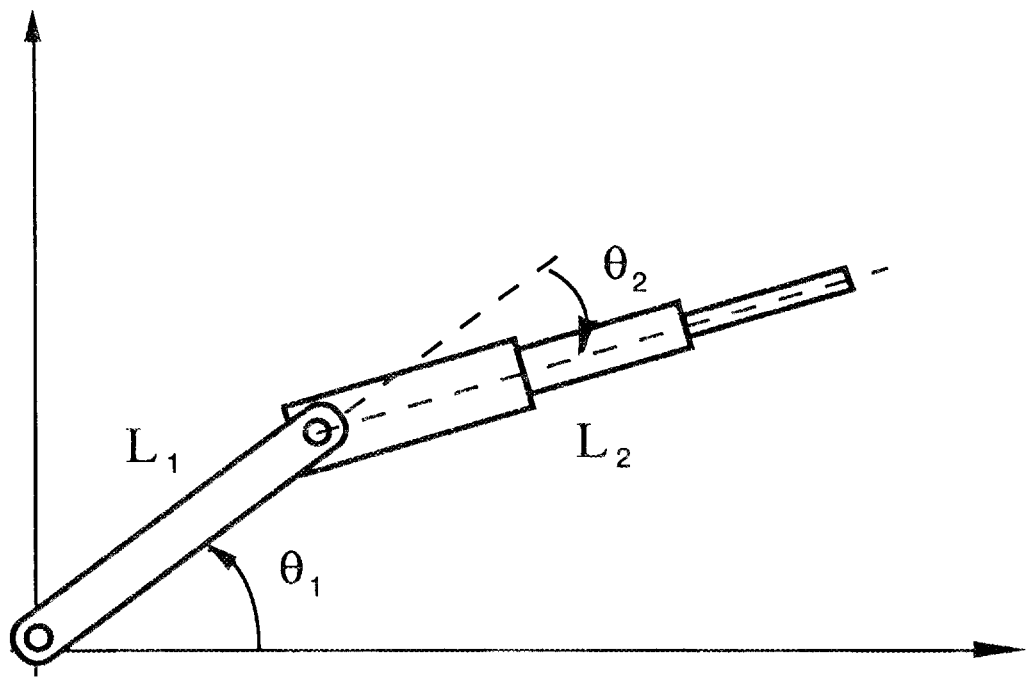

Fig. 9.17. Three-link planar robot to which an RPPE robot can be reduced to study its workspace.

Figure 9.18 shows the area covered by an RPPE when using only two discrete positions for the column and

$$\theta_{1max} = 40,$$
$$\theta_{1min} = -90,$$
$$\theta_{2max} = 0,$$
$$\theta_{2min} = -140°.$$

9.3.4.2 Conclusions for RPPE Manipulator Optimization

As in the case of the RPP manipulator, in order to assure that boundary singularities are not encountered, the total length of the manipulator must be greater than the diameter of the waste storage tank. A reasonable assumption would be approximately 110% of the diameter of the tank. In order to cover the top of the tank, it will be necessary to allow θ_2 to go through the zero position as with the RPP case.

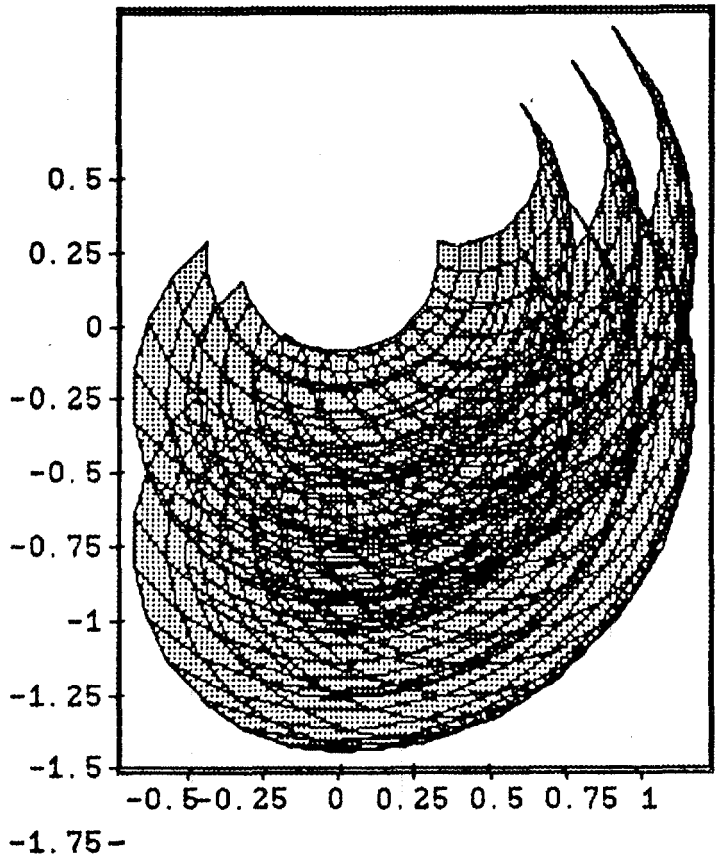

Fig. 9.18. Workspace of an RPPE robot with three stages for the second link and two discrete positions for the shoulder at (0, .25) and (0, -.25) and the height of the tank is equal to 1.

The angular constraints for the two pitch degrees of freedom are:

$$\theta_{1max} = 40,$$
$$\theta_{1min} = -90,$$
$$\theta_{2max} = 0,$$
$$\theta_{2min} = -140°.$$

Three stages of 80% extension are necessary for the extension link:

$$L_1 = 0.3,$$
$$L_{2min} = 0.29,$$
$$L_{2med} = 0.52,$$
$$L_{2max} = 0.7.$$

Only two discrete positions for the column at 25 and -25% of the height of the tank allow full coverage of the tank with the manipulator.

This configuration with an extra degree of freedom covers the workspace area with only two discrete positions for the column. This is the principal advantage because the movement of the column will not be as easy as with the other joints. Another advantage is that, due to the additional redundancy, more possibilities are added to robot path planing, making it possible to create some rectilinear movements that otherwise would be difficult to accomplish. But the RPPE configuration does not have a significant advantage in workspace coverage and complicates the robot with an extra degree of freedom.

9.3.5 Conclusions of the Kinematic Configuration Study

The study in Sect. 9.3 only considered positioning within the workspace. Conclusions cannot be drawn from only this type of study; however, it is fundamental to the conceptual design. If the workspace is constrained to the height of the waste tank liner (essentially the height of the cylindrical portion of the tank) and access to the roof domed area is not required, then the ERPP and the ERPPE manipulators appear, at first, to cover the workspace better, (as long as the elbow of the manipulator can be positioned either up or down), than the ERPE manipulator. An ERPP or ERPPE manipulator which is constrained to an elbow-up configuration by the second pitch joint limits is likely to have difficulty in reaching the upper levels of the workspace due to elbow interference with the tank roof. However, in the elbow-down position, the manipulator may be constrained by the waste stored in the tank. This leads to the conclusion that the ERPE manipulator configuration may be the best choice of those considered, even though there is a nearly hemispherical volume near the center of the tank and near the surface of the lined portion of the tank which cannot be reached. In the study, it was assumed that the first pitch joint in all three cases could be as high as 25% of the height of the lined portion of the tank above that portion of the tank.

If access to the roof domed area is required, the ERPE manipulator is less acceptable. Approximately 50% of the roof area, for the case considered, could not be reached. However, the ERPP and ERPPE manipulators could reach the entire area of the roof.

One configuration which had not been considered may be worth further consideration. This would be an ERPRP manipulator, i.e., a manipulator with an additional roll joint between the two pitch joints. This would allow the redundancy required to place the arm in a somewhat

horizontal position when necessary to avoid interference with the roof of the tank and the surface of the waste. One possible disadvantage of this configuration would relate to obstacle avoidance due to the vertical risers in many of the tanks. A second disadvantage would be the additional complexity associated with the drive system.

In the above study it was assumed that the radius of the tank is equal to the height of the tank liner (the cylindrical portion of the tank). For waste storage tanks with other aspect ratios, slightly different results may be obtained; however, the basic conclusions are likely to hold. Another important issue is the height of the waste in the tank and the specific volume which must be covered in a given case. In many cases it may only be necessary to access the lower half of the volume of the tank.

This study did not analytically consider the problem of inserting the manipulator into the tank, given the constraint of a full tank, although some thought has been given to it. The ERPPE manipulator may have an advantage over the ERPE manipulator in that this manipulator might be lowered to the second pitch joint providing a short ERPE manipulator which could clear a hemispherical volume of radius equal to the maximum length of the second link. (A three-section extension can collapse to approximately 40% of it's maximum length, thus the minimum length of the ERPE link would be approximately 0.4 or 0.5 while that of the ER(P)PE lowered only to the second pitch joint would be approximately 0.2 or 0.25, which clears the maximum height of the waste in the tank.) This may provide the volume necessary for insertion of the remainder of the manipulator. Further study should consider the problem of inserting the manipulator and this possible solution.

9.4 OTHER CONSIDERATIONS CONCERNING FUNDAMENTAL KINEMATIC CONFIGURATIONS

There are many other considerations which should be taken into account when selecting a kinematic configuration. As stated in Sect. 4.2, the manipulators designed for waste tank remediation will be required to perform a variety of tasks. Each of the tasks can be expressed either in terms of position and orientation requirements or in terms of motion control and/or force/torque control requirements (or impedance control requirements).

A number of performance criteria for manipulators have been considered by various researchers particularly in the area of redundant manipulator control. Two of these criteria are velocity ratio and mechanical advantage **[Dubey,86]**. The first of is directly related to singularities within the workspace. Ideally, one would like to have the ability to move and apply

forces and torques symmetrically in all directions at any point in the workspace.

In addition, for certain types of tasks there may be advantages to approaching the work surface from a wide orientation range. Further study along these lines would require the definition of the wrist constraints and/or the definition of a small multi-degree-of-freedom manipulator to be mounted on the end of the long-reach manipulator.

The lowest natural frequency of a manipulator link is inversely proportional to the square of the length of the link when the links are treated independently. This means that the ERPE manipulator may have a response advantage when the end point is significantly inside the workspace boundary and the length of the link is reduced. In this condition, the manipulator is also likely to be stiffer due to the combination of link sections.

10. CONCLUSIONS AND FUTURE DIRECTIONS

DOE is currently engaged in an aggressive effort to reduce the generation of radioactive waste by-products and to remediate contaminated sites and facilities. One of the highest priority remediation areas is waste storage tanks. Many of the concepts envisioned for deployment of remediation tools in waste storage tanks rely on long-reach, high-capacity manipulator systems.

Long-reach manipulators with high aspect ratios behave fundamentally differently than typical industrial robots or servomanipulators due to structural flexibility. The basic relationships involved were developed for a clamped-free beam with a circular cross section, including deflection and natural frequency of the first mode of vibration. A more general study was performed, also, as noted below. Material properties (considering steel, aluminum, and titanium) had little effect on the results. From the literature, servo bandwidths will need to be 33 to 67% lower than the first mode frequency. Composite materials are unlikely to raise the lowest structural natural frequency by more than a factor of 3. Although a potential exists for improvement in damping characteristics through the use of composite materials, it is unlikely that such materials would be specified for long-reach manipulators (especially early prototypes) due to cost.

The general workspace requirements of a manipulator for waste tank remediation application were briefly discussed. A study of the effect of the number of access ports through which a manipulator could be inserted on the required maximum manipulator arm length concluded that for four ports rather than one, the length could be reduced by approximately 30%. Due to the length squared effect, the natural frequency would be approximately doubled discounting any advantage due to cross-sectional area reduction. In addition to positionally covering the workspace, the design of a manipulator for waste tank remediation should take into account the tasks to be performed which are not clearly defined at this point. Examples of possible tasks were discussed.

A survey of the literature was performed and discussed in terms of three broad categories: (1) open-loop trajectory planning, (2) trajectory following using sensory feedback, and (3) multiple control strategies.

A transfer function approach to the modeling and simulation of a single flexible link was developed. Tables of normalized pole locations and zero locations for various transfer functions were obtained. These results were compared with those from a modal analysis approach. The poles obtained from the two approaches for a specific example correlated well; however, the zeros for the joint torque input to end-point position output matched only at the first frequency. The discrepancies obtained have been

previously noted in the literature and remain an open issue. An advantage of the transfer function approach is that end-point forces and torques can be more easily handled.

Open-loop trajectory planning was subdivided into two distinct approaches, vibration suppression and inverse dynamic methods, for discussion. Vibration suppression approaches modify the actuator commands so that the resonant frequencies are not excited. The inverse dynamics approach uses the full dynamic model of the flexible manipulator to find the actuator command to achieve a desired motion trajectory. An extension to Kwon's work **[Kwon,91]** was developed which is its application to a specific class of trajectories which greatly simplifies the amount of computation required.

A classical feedback controller was designed using both hub and tip information. Classical methods were applied because of their historical acceptability in industry and the fact that a baseline to which the performance of other types of controllers can be compared would be established. It appears that improvements in the bandwidth of a flexible manipulator will be difficult to obtain with classical controllers. Advancements in sensor, actuator, and controller design will be necessary to significantly improve the bandwith of flexible manipulators.

The potential types of actuators for a manipulator for waste storage tank remediation were briefly discussed with the conclusion that hydraulic cylinders would be assumed. The workspace of a manipulator is directly affected by the range of motion of the joints. Therefore, a study was conducted to determine the optimum joint linkage configuration having a maximum joint angle range for a given minimum actuation torque throughout the joint range (a relatively constant actuation torque throughout the joint range is most desirable). It was determined that if a hydraulic cylinder is used as an actuator of a revolute joint and that no additional mechanisms or drives are included, a reasonable joint motion constraint would be approximately 135°, which correlates with typical industrial applications.

A study of the positioning workspaces of three potential manipulator configurations was conducted to determine the one most applicable to the waste storage tank remediation problem. The manipulator configurations selected for study included an extend-roll-pitch-pitch manipulator, an extend-roll-pitch-extend manipulator, and an extend-roll-pitch-pitch-extend manipulator, discounting the wrist degrees of freedom. For situations in which it is not necessary for the manipulator to reach the top of the tank or the area above the cylindrical portion of the tank, the extend-roll-pitch-extend configuration appeared to be best. One apparent advantage is that the elbow position of the other manipulators considered may be difficult to

accommodate for some portions of the workspace and levels of waste in the tank. However, for situations in which it is necessary to reach the tank roof, the extend-roll-pitch-pitch-extend manipulator may be a better choice as long as it is possible to move the second pitch joint through the zero position to produce both elbow-up and elbow-down configurations.

It should be noted that the problem of "snaking" the manipulator into a tank which is full and which is cluttered was not analytically addressed in this initial study, although several solutions to the problem have been identified. The extend-roll-pitch-pitch-extend manipulator may have an advantage in performing work near the center of the tank. Using only the extend, roll, second pitch, and final extend may provide clearance to allow the remainder of the manipulator to be inserted into the tank. More complex manipulators such as an extend-roll-pitch-extend-pitch-extend manipulator or manipulators with changeable links of different lengths are other options.

The selection of a manipulator configuration should not be made based only on the positioning workspace coverage, although it is fundamental to the problem. A brief discussion of other selection criteria which relate manipulator performance to the performance of tasks was included.

Future directions in the study of long-reach manipulation include additional kinematic and dynamic analysis and experimental verification of the algorithms developed. In the kinematic analysis area, the implications of inserting the arm into a tank need to be addressed as well as those of specific task requirements. The studies conducted in FY 1991 and discussed in this report did not consider these additional requirements. The level of waste in specific tanks and the volumetric coverage actually needed could also impact the particular kinematic configuration selected.

In the dynamic modeling, analysis, and controls area, the dynamics and controls implications of specific task requirements need to be addressed. Multi-degree-of-freedom models of manipulators to be considered are needed for multi-body dynamics and controls studies. Plans are to obtain general purpose software developed for this type of work. In addition, plans include the experimental verification of control algorithms developed in FY 1991 on a single-degree-of-freedom test stand and additional algorithm development.

REFERENCES

[Asada,90] Asada, H., Park, J. H., and Rai, S., "A Control-Configured Flexible Arm: Integrated Structure/Control Design," Proc. of 1991 IEEE International Conference on Robotics and Automation, Sacramento, Calif., April 9-11, 1991, Vol. III, pp. 2356-62.

[Bayo,87a] Bayo, E. "A Finite-Element Approach to Control the End-Point Motion of a Single-Link Flexible Robot, *Journal of Robotic Systems* 4(1), pp. 63-75 (1987).

[Bayo,87b] Bayo, E., and Paden, B., "On Trajectory Generation for Flexible Robots," *Journal of Robotic Systems* 4(2), pp. 229-35 (1987).

[Bayo,89] Bayo, E., and Moulin, H., "An Efficient Computation of the Inverse Dynamics of Flexible Manipulators in the Time Domain," 1989 IEEE (International Conference on Robotics and Automation), pp. 710-15.

[Blevins,79] Blevins, R. D., *Formulas for Natural Frequency and Mode Shape*, Van Nostrand, New York, 1979.

[Book,83] Book, W. J., and Majette, M., "Controller Design for Flexible, Distributed Parameter Mechanical Arms Via Combined State Space and Frequency Domain Techniques," *Journal of Dynamic Systems, Measurement, and Control*, Vol. 185, pp 245-54, (December 1983).

[Book,90] Book, W. J., and Kwon, D. S., "Contact Control for Advanced Applications of Light Weight Arms," in UTA ARRI CRAM, 1990.

[Cannon,84] Cannon, Jr., R. H., and Schmitz, E., "Initial Experiments on the End-Point Control of a Flexible One-Link Robot," *Int. Robotics Research*, 3(3), pp. 62-75 (Fall 1984).

[Cetinkunt,90a] Cetinekunt, S., and Book, Wayne. J., "Performance Limitations of Joint Variable-Feedback Controllers Due to Manipulator Structural Flexibility," *IEEE Trans. Robotics and Automation*, 6(2) (April 1990).

[Cetinekunt,90b] Cetinekunt, S. and Wu, S.,"Tip Position Control of a Flexible One Arm Robot with Predictive Adaptive Output Feedback Implemented with Lattice Filter Parameter Identifier," Proc. of 1990 IEEE International Conference on Robotics and Automation, Cincinnati, Ohio, May 13-18, 1990, pp. 1620-25.

[Cetinekunt,91] Cetinekunt, S., and Yu, W., "Closed-Loop Behavior of a Feedback-Controlled Flexible Arm: A Comparative Study," *Int. Robotics Research*, 10 (3), pp. 263-75 (June 1991).

[Chalhoub,86] Chalhoub, N. G., and Ulsoy, A. G., "Dynamic Simulation of a Leadscrew Driven Flexible Robot Arm and Controller," *J. Dynamic Syst., Meas. and Control*, 108, pp. 119-26 (June 1986).

[Chen,90] Chen, Jian-Shiang and Chia-Hsiang Menq, "Experiments on the Payload-Adaption of a Flexible One-Link Manipulator with Unknown Payload," Proc. of 1990 IEEE International Conference on Robotics and Automation, Cincinnati, Ohio, May 13-18, 1990, pp. 1614-19.

[Chiang,91] Chiang, W. W., Kraft, R. and Cannon, R. H. Jr., "Design and Experimental Demonstration of Rapid, Precise End-Point Control of a Wrist Carried by a Very Flexible Manipulator," *International Journal of Robotics* Research, Vol. 10, No. 1, pp. 30-40, (1991).

[Christian,90] Christian, A. D., and Seering, Warren, P., "Initial Experiments with a Flexible Robot," Proc. of 1990 IEEE International Conference on Robotics and Automation, Cincinnati, Ohio, May 13-18, 1990, pp. 722-27.

[Chew,89] Chew, K. K., and Tomizuka, M., "Digital Control of Repetitive Errors in Disk Drive Systems," Proc. Amer. Cont. Conf., pp. 540-48, 1989.

[De Maria,87] De Maria, Giuseppe and Siciliano, B., "A Multilayer Approach to Control of a Flexible Arm," Proc. of 1987 IEEE International Conference on Robotics and Automation, 1987, pp. 774-78.

[Dubey,86] Dubey, R. V., *Analysis and Control of Redundant Robots*, Dissertation, Clemson University, Dec. 1986.

[Dubowsky,87] Dubowsky, S., and Tanner, A. B., "A Study of the Dynamics and Control of Mobile Manipulators Subjected to Vehicle Disturbances," Proc. of the Fourth International Symposium of Robotics Research at Santa Cruz, Calif., Aug. 9-14, 1987.

[Feliu] Feliu, V., Rattan, K. S., and Brown, H. B., "Adaptive Control of a Single-Link Flexible Manipulator in the Presence of Joint Friction and Load Changes," pp. 1036-1039, in *Proc. of 1989 IEEE International Conference on Robotics and Automation*, Scottsdale, Arizona, May 1989.

[Good,85] Good, M. C., Sweet, L. M., and Strobel, K. L., "Dynamic Models for Control System Design of Integrated Robot and Drive Systems," *J. of Dynamic Syst., Meas., and Control*, 107, pp. 53-59 (March 1985).

[Goodson,70] Goodson, R. E., "Distributed System Simulation Using Infinite Product Expansions," Simulation, Dec. 1970, pp. 255-63.

[Hara,88] Hara, S., Yamamoto, Y., Omata, T., and Nakano, M., "Repetitive Control System: A New Type Servo System for Periodic Exogenous Signals," *IEEE Transactions on Automatic Control*, Vol. 33, No. 7, pp. 659-67 (July 1988).

[Hastings,86] Hastings, G. G., and Book, W. J., "Verification of a Linear Dynamic Model for Flexible Robotic Manipulators," pp. 1024-29, in *Proc. 1986 IEEE International Conference on Robotics and Automation*, San Francisco, Calif. April 1986.

[Higdon,76] Higdon, A., et al. *Mechanics of Materials*, Wiley, New York, 1976.

[Hyde,91] Hyde, J. M., and Seering, W. P., "Using Input Command Pre-Shaping to Suppress Multiple Mode Vibration," Proc. of 1991 IEEE International Conference on Robotics and Automation, Sacramento, Calif., April 9-11, 1991, Vol. III, pp. 2604-11.

[Jones,88] Jones, J. F., and Petterson, B. J., "Oscillation Damped Movement of Suspended Objects," 1988 IEEE International Conf. on Robotics and Automation, Philadelphia, Penna., April 25, 1988.

[Korolov,89] Korolov, V.V. and Chen Y. H., "Controller Design Robust to Frequency Variation in a One-Link Flexible Robot Arm," *Journal of Dynamic Systems, Measurement, and Control*, Vol. 111 pp. 9-14 (March 1989).

[Kotnik,88] Kotnik, P. T., Yurkovich, S. and Ozguner, O., "Acceleration Feedback for Control of a Flexible Manipulator Arm," *Journal of Robotic Systems*, 5(3), pp. 181-96, (1988).

[Kwon,90] Kwon, D. S. and Book, W. J., "An Inverse Dynamic Method Yielding Flexible Manipulator State Trajectories," Proc. of 1990 American Control Conference.

[Kwon,91] Kwon, D. S., *An Inverse Dynamic Tracking Control for Bracing a Flexible Manipulator*, Ph.D Thesis, School of Mechanical Engineering, Georgia Institute of Technology, June, 1991

[Lee,90] Lee, H. G., Kawamura, S., Miyazaki, F. and Arimoto, S., "External Sensory Feedback Control for End-effector of Flexible Multi-Link Manipulators," Proc. of 1990 IEEE International Conference on Robotics and Automation, Cincinnati, OH, May 13-18, 1990, pp. 1796-1802.

[LePage,61] LePage, W. R., *Complex Variables and the Laplace Transform for Engineers*, Dover Publications, Inc. New York, pp. 285-335, 1961.

[Lew,90] Lew, J. Y., and Book, W. J., "Control and Applications of Cooperating Disparate Robotic Manipulators Relevant to Nuclear Waste Management," in *Proceedings of the 38th Conference of Remote Systems Technology,* Nashville, Tenn., Vol. 2, 1990.

[Mecki,90] Mecki, P. H., and Seering, W. P., "Experimental Evaluation of Shaped Inputs to Reduce Vibration for a Cartesian Robot," *J. Dynamic Systems, Measurement, and Control,* 112, pp. 159-65 (June 1990).

[Menq,88] Menq, C. H. and Chen, J. S., "Dynamic Modeling and Payload-Adaptive Control of a Flexible Manipulator," 1988 IEEE (International Conference on Robotics and Automation), pp. 488-93.

[Merritt,67] Merritt, H. E., *Hydraulic Control Systems,* Wiley, New York, 1967.

[Miu,90] Miu, D. K., *Physical Interpretation of Transfer Function Zeros for Simple Control Systems with Mechanical Flexibilities,* Report 90-08, Univ. of Calif. at Los Angeles, April 1990.

[Nelson,86] Nelson, W. L., and Mitra, D., "Load Estimation and Load-Adaptive Optimal Control for a Flexible Robot Arm," 1986 IEEE (International Conference on Robotics and Automation), pp 206-11.

[Noakes,90] Noakes, M. W., Petterson, B. J., and Werner, J. C., "An Application of Oscillation Damped Motion for Suspended Payloads to the Advanced Integrated Maintenance System," in *Proceedings of the 38th Conference of Remote Systems Technology,* Nashville, Tenn., 1990.

[Park,90] Park, J. H. and Asada, H., "Design and Control of Minimum-Phase Arms with Torque Transmission Mechanisms," Proc. of 1990 IEEE International Conference on Robotics and Automation, Cincinnati, OH, May 13-18, 1990, pp. 1790-95.

[Petterson,90] Petterson, B. J., Robinett, R. D., and Werner, J. C., "Parameter-Scheduled Trajectory Planning for Suppression of Coupled Horizontal and Vertical Vibrations in a Flexible Rod," Proc. of 1990 IEEE International Conference on Robotics and Automation, Cincinnati, Ohio, May 13-18, 1990, pp. 916-21.

[Press,86] Press, W. H., Flannery, B. P., Teukolsky, S. A., and Vetterling, W. T., *Numerical Recipes,* Cambridge University Press, New York, 1986.

[Sakawa,85] Sakawa, Y., Matsuno, F., and Fukushima, S., "Modeling and Feedback Control of a Flexible Arm," *Journal of Robotic Systems* 2(4), pp. 453-72, (1985).

[Schoenwald,91] Schoenwald, D. A., et. al., "Minimum-Time Trajectory Control of a Two-Link Flexible Robotic Manipulator," Proc. IEEE Inter. Conf. on Robotic and Automation, Sacramento, Calif., April 1991.

[Serna,90] Serna, M. A. and Bayo, E., "Trajectory Planning for Flexible Manipulators," Proc. of 1990 IEEE International Conference on Robotics and Automation, Cincinnati, Ohio, May 13-18, 1990, pp. 910-15.

[Siciliano,88] Siciliano, B., and W. J. Book, "A Singular Perturbation Approach to Control of Lightweight Flexible Manipulators," *The International Journal of Robotics Research*, Vol. 7, No. 4, August 1988.

[Singer,88] Singer, N. C., Seering, W. P., "Using Acausal Shaping Techniques to Reduce Robot Vibration," 1988 IEEE (International Conference on Robotics and Automation), pp 1434-39.

[Singhose, 90] Singhose, W. E., Seering, W. P., and Singer, N. C., "Shaping Inputs to Reduce Vibration: A Vector Diagram Approach," Proc. of 1990 IEEE International Conference on Robotics and Automation, Cincinnati, Ohio, May 13-18, 1990, pp. 922-27.

[Spector,90] Spector, V. A., and Flashner, H., "Modeling and Design Implications of Noncollocated Control in Flexible Systems," *J. Dynamic Syst., Meas., and Control*, 112, pp. 187-93 (June 1990).

[Tzes,90] Tzes, A. P., and Yurkovich, S.,"A Frequency Domain Identification Scheme for Flexible Structure Control," *Journal of Dynamic Systems, Measurement, and Control*, Vol. 112, pp. 427-34 (September 1990).

[Vinke,91] Vinke, D., and Vidyasagar, M., "New Techniques for H_2 Optimal Control of a Flexible Beam", Proc. of 1991 IEEE International Conference on Robotics and Automation, Sacramento, Calif., April 9-11, 1991, Vol. III, pp. 2592-97.

[Wang,89] Wang, W. J., Lu, S. S. and Hsu, C. F. "Experiments on the Position Control of a One-Link Flexible Robot Arm," *1989 IEEE Transactions on Robotics and Automation*, Vol. 5, No. 3, pp. 373-77 (June 1989).

[Weaver,90] Weaver, W., Timoshenko, S. P., and Young, D. H., *Vibration Problems in Engineering*, Wiley, New York, 1990.

[West,a] West, H., and Asada, H., "Design and Analysis of Braced Manipulators for Improved Stiffness," Proc., Third ISRP Conference, Chantilly, France.

[West,b] West, H., and Asada, H., "Kinematic Analysis and Mechanical Advantage of Manipulators Constrained by Contact with the Environment," Proc., ASME Winter Annual Meeting, Miami, Fla.

[Yuan,89a] Yuan, B., "Adaptive Strategies for Controls of Flexible Arms," Ph.D. dissertation, Georgia Institute of Technology, 1989.

[Yuan,89b] Yuan, B., Book, W. J., and Siciliano, B., "Direct Adaptive Control of a One-Link Flexible Arm with Tracking," *J. Robotic Systems*, 6(6) pp. 663-80 (1989).

[Yuh,89] Yuh, J., Young, T., and Baek, Y. S., "Modeling of a Flexible Link Having a Prismatic Joint in Robot Mechanism – Experimental Verification," pp 722-727, in *Proc. of 1989 IEEE International Conference on Robotics and Automation*, Scottsdale, Arizona, May 1989.

[Yuh,90] Yuh, J., "Application of Discrete-Time Model Reference Adaptive Control to a Flexible Single-Link Robot," *Journal of Robotic Systems*, 4(5), pp 621-30 (1987).

[Yurkovich,90] Yurkovich, S., Tzes, A. P., Lee, I., and Hillsley, K. L., "Control and System Identification of a Two-Link Flexible Manipulator," Proc. of 1990 IEEE International Conference on Robotics and Automation, Cincinnati, Ohio, May 13-18, 1990, pp. 1626-31.

[Zalucky,84] Zalucky, A., and Hardt, D. E., "Active Control of Robot Structure Deflections," *Journal of Dynamic Systems, Measurement, and Control*, Vol. 106, pp. 63-69 (March 1984).

INTERNAL DISTRIBUTION

1. G. A. Armstrong
2-21. S. M. Babcock
22. W. D. Burch
23. B. L. Burks
24. P. L. Butler
25. H. M. Costello
26. S. S. Douglass
27. M. J. Haire
28. D. C. Haley
29. W. R. Hamel
30. J. F. Jansen
31. R. K. Kibbe
32. R. L. Kress
33. D. S. Kwon
34. A. P. Malinauskas
35. R. C. Mann
36. S. March-Leuba
37-39. S. A. Meacham
40. F. G. Pin
41. K. E. Plummer
42. B. S. Richardson
43. J. C. Rowe
44. J. E. Rutenber
45. S. L. Schrock
46-47. Laboratory Records Department
48. Laboratory Records ORNL-RC
49. Document Reference Section
50. Central Research Library
51. ORNL Patent Section
52-53. RPSD Publications Office

EXTERNAL DISTRIBUTION

54. Office of Assistant Manager for Energy Research and Development, DOE Field Office, Oak Ridge, P. O. Box 2008, Oak Ridge, TN 37831.
55. G. A. Armantrout, Lawrence Livermore National Laboratory, 7000 East Avenue, L-440, Livermore, CA 94550.

56. D. W. Bennett, Pacific Northwest Laboratories, P. O. Box 999, Richland, WA 99352.
57. T. Beugelsdjik, Los Alamos National Laboratories, P. O. Box 1663, MS J-580, Los Alamos, NM 87545.
58. W. J. Book, Georgia Institute of Technology, The George W. Woodruff School of Mechanical Engineering, Atlanta, GA 30332.
59. R. Craig, Commander, U.S. Army Toxic and Hazardous Materials Agency, ATTN: CETHA-TS-S, Aberdeen Proving Ground, MD 21010-5401
60. P. J. Eicker, Sandia National Laboratories, P. O. Box 5800, Division 1410, Albuquerque, NM 87185.
61. M. Evans, Pacific Northwest Laboratories, P. O. Box 999, Battelle Boulevard, MS K5-22, Richland, WA 99352.
62. J. Feddema, Sandia National Laboratories, P. O. Box 5800, Division 1414, Albuquerque, NM 87185.
63. B. Griebenow, EG&G Idaho, Inc., P. O. Box 1625, Idaho Falls 83415-3415
64. R. W. Harrigan, Sandia National Laboratories, P. O. Box 5800 Division 1414, Albuquerque, NM 87185.
65. D. L. Jacoboski, Westinghouse Environmental Management Company of Ohio, P. O. Box 398704, Cincinnati, OH 45239-8704.
66. L. M. Martinson, Westinghouse Idaho Nuclear Company, P. O. Box 4000, Idaho Falls, ID 83403-5104.
67. H. McClelland, U.S. Army Human Engineering Laboratory, ATTN: SLCHE-CS, Building 459, Aberdeen Proving Ground, MD 21005-5001.
68. J. Pennington, Automation Technology Branch, Information Sciences Division, NASA Langley Research Center, MS 152-D, Hampton, VA 23665-5225.
69. C. M. Shoemaker, Advanced Systems Concept Offices (ASCO), ATTN: AMSLC-AT-AS, Building 459, Aberdeen Proving Ground, MD 21005-5001.
70. C. R. Ward, Westinghouse Savannah River Company, Building 773-A D-1145, Aiken, SC 29808.
71. A. P. Williams, Department of Energy, 12800 Middlebrook Road, MS EM-55, Trevion II, Germantown, MD 20874.
72. L. W. Yarbrough, Department of Energy, MS EM-55, Trevion II/Suite 400, Germantown, MD 20874.
73. J. A. Yount, Westinghouse Hanford Company, P. O. Box 1970, MSIN LO-18, Richland, WA 99352.

74-83. Office of Scientific and Technical Information, P. O. Box 62, Oak Ridge, TN 37831.